

Interactions Between Fast and Slow Dynamics in Nonlinear Evolution Equations

JKT

December 17, 2018

Contents

| | | |
|----------|---|-----------|
| 1 | Introduction | 1 |
| 1.1 | Reduced Dynamics | 3 |
| 2 | Geometric Singular Perturbation Theory | 4 |
| 3 | Singularities and Fold Points | 5 |
| 3.1 | Fold Points in the Van der Pol System | 6 |
| 3.1.1 | Extended System | 7 |
| 4 | The Blow-Up Method | 7 |
| 4.1 | Coordinate Transformation and Charts | 8 |
| 4.2 | Dynamics in K_2 | 10 |
| 4.3 | Dynamics in K_1 | 12 |
| 4.4 | Dynamics in K_3 | 15 |
| 4.5 | The Full Solution | 18 |
| 5 | Canard in Two Dimensions | 18 |
| 5.1 | Canard Blow-up | 21 |
| 5.1.1 | Dynamics in K_2 | 22 |
| 5.1.2 | Dynamics in K_1 | 24 |
| 5.2 | Effect of the Canard Point | 25 |
| 5.2.1 | Separation of the Manifolds | 27 |
| 6 | Canards in Three Dimensions | 28 |
| 6.1 | The Folded Node | 32 |
| 7 | MMO | 35 |
| 7.1 | The Folded Node | 39 |
| 8 | Discussion/Conclusion | 43 |
| 9 | Acknowledgements | 43 |
| A | Elements of Dynamical Systems | 45 |
| A.1 | Stable Manifold Theorem | 45 |
| A.2 | Centre Manifold Theorem | 45 |
| A.3 | Implicit Function Theorem | 45 |
| A.4 | Hartman Grobman Theorem | 45 |
| A.5 | Hopf Bifurcations | 45 |
| B | Numerical Simulation | 45 |
| B.1 | Stiff Solvers | 48 |
| C | Dynamics in K_2 | 48 |

List of Figures

| | | |
|----|--|----|
| 1 | Examples of fast-slow systems in nature (neuron,ECG etc.) | 1 |
| 2 | Van der Pol Dynamics with $\epsilon = 1$ | 2 |
| 3 | Van der Pol Dynamics with $\epsilon = 0.01$ | 3 |
| 4 | Three charts mapping different sections of our blow up (Krupa & Szmolyan 2001). | 8 |
| 5 | Phase portrait for chart 2 (Krupa & Szmolyan 2001) | 10 |
| 6 | Riccati solution for chart 2 (Krupa & Szmolyan 2001) | 11 |
| 7 | Dynamics in chart 1 (Krupa & Szmolyan 2001) | 13 |
| 8 | Flow on the Van der Pol system. | 18 |
| 9 | The reduced flow where a) $\lambda = 0$ and b) $\lambda > 0$ | 19 |
| 10 | The Van der Pol system for the canard case. | 21 |
| 11 | The trajectories associated with the canards case of the Van der Pol system. | 26 |
| 12 | Separation of M_a and M_r (Kuehn 2015). | 27 |
| 13 | Three dimensional Van der Pol (Festschrift et al. 2001). | 29 |
| 14 | Phase portraits of our three dimensional system where a) is a folded saddle, b) folded node, c) and d) are desingularised flows (Desroches et al. 2012). | 31 |
| 15 | The branches of a spiral (International Technological University n.d.). | 31 |
| 16 | Three dimensional Van der Pol (Festschrift et al. 2001). | 36 |
| 17 | Phase portraits of our three dimensional system where a) is a folded saddle, b) folded node, c) and d) are desingularised flows (Desroches et al. 2012). | 38 |
| 18 | The branches of a spiral (International Technological University n.d.). | 38 |
| 19 | Folded Node Region for $\mu \approx 0.0557$. (Desroches et al. 2012). | 42 |
| 20 | Rotational Sectors for $\mu \approx 0.0557$ (Desroches et al. 2012). | 42 |
| 21 | Numerical Stability Comparison | 47 |
| 22 | Stiff Solvers | 48 |

Abstract

This project will be considering the Fast-Slow dynamics in non-linear ordinary differential equations. The project will start by considering the theory associated with Fast-Slow dynamical systems such as Geometric Perturbation Theory (Section 2). Then the project moves onto two-dimensional systems by first looking at the general form, using [Krupa & Szmolyan \(2001\)](#) theory (Section 1), before applying it to the Van der Pol system (Section ??). From here the project will also consider the non-hyperbolicity of the fold points present in the system, where a jump might occur (Section 4). Once the fold point has been ‘blown-up’ for the normal case, it is prudent to consider the canard system - where the parameter λ is introduced. This could cause a split within the manifolds or a Hopf bifurcation could occur causing a periodic solution (Sections 5 and 5.2.1). Once this has been considered, the next step is to consider the Fast-Slow system in a three dimensional case for folded singularities (Section 6) before continuing onto the theory behind Mixed Mode Oscillations (Section ??). **Lastly, the project will discuss the numerical simulations associated with the construction of the models and the results obtained.**

1 Introduction

+++Motivate motivate motivate+++

Nonlinear evolution equations ubiquitous across the sciences. These typically take the form

$$\dot{x}(t) = F(x(t))$$

where $x \in \mathbf{R}^d, F \in C^r(\mathbf{R}^d, \mathbf{R}^d)$. We will be interested in systems that occur on different timescales, known as fast-slow systems. These occur naturally in physics, neuroscience and many other biological scenarios +++ Van der Pol, FitzHugh-Nagumo, other bio ref?+++. Models of such systems can be written generally in the form given below.

$$\begin{cases} x' = \frac{dx}{dt} = f(x, y, \epsilon), \\ y' = \frac{dy}{dt} = \epsilon g(x, y, \epsilon), \end{cases} \quad (1)$$

Here, $x \in \mathbf{R}^n, y \in \mathbf{R}^m, m, n \geq 1$ and f, g are sufficiently smooth. The separation in timescales is governed by $0 < \epsilon \ll 1$, known as the timescale separation parameter. Some systems also act on more than two timescales, in which case there is more than one timescale separation parameter. In the system above, note that the change in x is $O(1)$, whilst it is $O(\epsilon)$ in y . As ϵ is very small, this means that the change in x is much faster than that of y . If we slow down time with the transformation $\tau = \epsilon t$, the system becomes

$$\begin{cases} \epsilon \dot{x} = \epsilon \frac{dx}{d\tau} = f(x, y, \lambda, \epsilon), \\ \dot{y} = \frac{dy}{d\tau} = g(x, y, \lambda, \epsilon), \end{cases} \quad (2)$$

Represented like this, $\dot{x} = O(\frac{1}{\epsilon})$ whilst $\dot{y} = O(1)$. The time scale given by τ is said to be slow so (2) is the *slow system* while (1) is the *fast system*.

Figure 1: Examples of fast-slow systems in nature (neuron,ECG etc.)

Throughout what follows, the motivating example will be the Van der Pol equation. The Van der Pol oscillator is a well-studied second order ODE that is used to model a variety of physical and biological phenomena. It

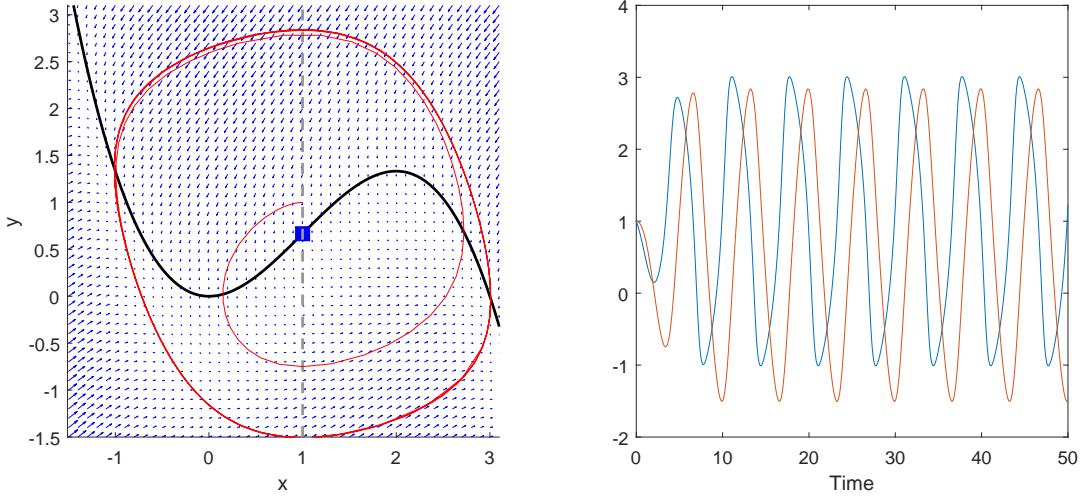


Figure 2: Phase plane and time series of the Van der Pol for $\epsilon = \lambda = 1$ started from $(1, 1)$. The dashed line indicates the null cline in y while that in x is given by the solid black line. The equilibrium is highlighted in blue.

was developed by the Dutch physicist and electrical engineer Balthasar Van der Pol, who conducted research on electrical circuits. It describes the evolution of the position coordinate $x(t)$ according to the following the ODE:

$$\ddot{x}(t) - \mu(1 - x^2(t))\dot{x}(t) + x(t) = 0, \quad (3)$$

where $\mu \gg 1$ is a scalar constant. This equation can be scaled so that it becomes a two dimensional fast-slow system of the form shown in Equation (1) after a change of variables.

$$\begin{aligned} x' &= -y + x^2 - \frac{x^3}{3} \\ y' &= \epsilon(-\lambda + x) \end{aligned} \quad (4)$$

When presented with any dynamical system, the aim is to fully understand the global dynamics of the system. A numerical simulation is often a good first step. Setting $\lambda = \epsilon = 1$ gives the phase plane given in Figure 2. Figure 2 shows the presence of a periodic large amplitude oscillation, which Van der Pol called *relaxation oscillations*. Setting $\epsilon = 1$ means that there is no separation in timescale. Figure 3 shows a more realistic scenario, when $\epsilon = 0.01$. Here there is what appears to be an almost instantaneous change in x every 800 time steps. What causes this rapid change? We wish to find a rigorous reason for this jump from slow to fast movement. A natural starting point would be to study what happens when $\epsilon = 0$, that is, when this rapid change is in fact instantaneous. Doing so in both the fast and slow system will give two different views of the dynamics. Taking the limit $\epsilon \rightarrow 0$ in the fast system (1) gives,

$$\begin{cases} x' &= \frac{dx}{dt} = f(x, y, \lambda, \epsilon) \\ y' &= 0. \end{cases} \quad (5)$$

This is known as the *layer problem* as movement is restricted to the layers $y = \text{const.}$ and similarly taking the

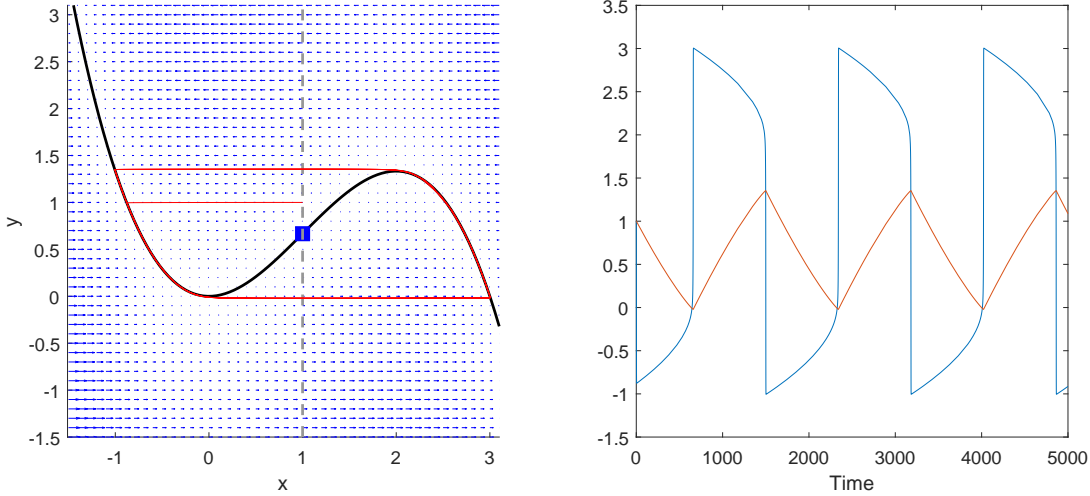


Figure 3: Phase plane and time series of the Van der Pol for $\epsilon = 0.01, \lambda = 1$ started from $(1, 1)$. The dashed line indicates the null cline in y while that in x is given by the solid black line. The equilibrium is highlighted in blue.

limit in the slow system (2) gives

$$\begin{cases} 0 &= \epsilon \frac{dx}{d\tau} = f(x, y, \lambda, 0) \\ \dot{y} &= \frac{dy}{d\tau} = g(x, y, \lambda, 0). \end{cases} \quad (6)$$

This is known as the *reduced problem* as the dynamics are reduced from the whole plane to the line $f = 0$. In the Van der Pol system, $f(x, y, \lambda, \epsilon) = -y + x^2 + \frac{x^3}{3}$ and $g(x, y, \lambda, \epsilon) = -\lambda + x$. The set $S = \{(x, y) : f(x, y, 0) = 0\} = \left\{(x, y) : y = x^2 - \frac{x^3}{3}\right\}$ is called the *critical manifold*. We thus have two separate systems that combine to illustrate the global dynamics when $\epsilon = 0$ and $\lambda = 1$. It remains to show that the flow in these limiting cases persists under perturbation to $0 < \epsilon \ll 1$ and ascertain whether the behaviour is the same for all λ . We shall restrict our attention to the jump at $(x_0^1, y_0^1) = (0, 0)$, the case for the point $(x_0^2, y_0^2) = (2, \frac{4}{3})$ is analogous. The aim is to fully understand the dynamics in a neighbourhood of these jump points for $\epsilon \ll 1$.

1.1 Reduced Dynamics

In order to determine the reduced dynamics on the critical manifold S , we consider the reduced problem (6). The critical manifold is an S-shaped curve. Since the flow on S is determined by \dot{y} , it can be seen that since the sign of g is negative in the neighbourhood of the jump point $(0, 0)$, the slow flow on S is directed towards this point.

The two jump points $(x_0^{1,2}, y_0^{1,2})$ coincide with the extrema of the cubic function $\phi(x) = y = x^2 - \frac{x^3}{3}$. Then using the chain rule, we can express the change in x using the second Equation of 6 as,

$$\phi_x(x)\dot{x} = g(x, \phi(x), 0). \quad (7)$$

Rearranging this gives an expression for the dynamics in x on S . We find that $\phi(x) = x^2 - \frac{x^3}{3}$, where the

derivative with respect to x gives $\phi_x(x) = 2x - x^2$. Therefore Equation 7 becomes

$$\dot{x} = \frac{g(x, \phi(x), 0)}{\phi_x(x)} = \frac{x-1}{2x-x^2} = \frac{x-1}{x(2-x)}.$$

The reduced dynamics are singular at $x = 0$ and $x = 2$. Therefore, no conclusions about the dynamics of x can be made at the jump points in this system.

The dynamics in the layer problem (5) are simpler. In this system, the manifold S contains all the equilibrium points. Whatever the initial data, the position moves horizontally towards S at which point it stops. The issue of reconciling the reduced and layer problems is considered using geometric singular perturbation theory (GSPT) in Section 2, along with conditions for the persistence of the dynamics under perturbation in ϵ . However, this will not cover the singularities. The reasoning for this is given in Section 3. The blow up method is employed in Section 4 to address the singularities. The case when $\lambda \neq 1$ is considered in Section 5 while Section 6 then begins to look at higher dimensional fast-slow systems.

2 Geometric Singular Perturbation Theory

The main question GSPT aims to answer is the following: under what conditions can it be concluded that the dynamics on the critical manifold $S = S_0$, persist as an invariant manifold S_ϵ under a small perturbation $0 < \epsilon \ll 1$? In higher than 2 dimensions the idea of transversality of the flow of the stable and unstable manifolds is essential for analysis, while in 2 dimensions this is rather trivial (Desroches et al. 2012). The main contribution to GSPT comes from Fenichel (1979) and his three theorems can be summed up in one, according to (Desroches et al. 2012). However, before stating the theorem, some formal definitions are needed.

Definition 2.1. Normal Hyperbolicity (Hek 2009)

A submanifold $M \subseteq S$ is called normally hyperbolic, if the Jacobian $\frac{\partial f}{\partial x}(x, y, \lambda, 0)$, where $(x, y) \in M$, has only eigenvalues with nonzero real part.

Moreover, the points $(x, y) \in M$, M normally hyperbolic, are hyperbolic equilibria of Equation 5 (Desroches et al. 2012). A normally hyperbolic submanifold can be classified according to its stability property: If M only has eigenvalues with positive real part it is called repelling, otherwise eigenvalues with negative real part are called attracting and if M is neither attracting nor repelling it is called a saddle-type submanifold (Desroches et al. 2012). Furthermore, stable and unstable manifolds can be defined as $W^s(M)$ and $W^u(M)$, corresponding to the eigenvalues with negative and positive real part, respectively. Now, with the following definition it is established which notion of distance is going to be employed throughout this analysis.

Definition 2.2. Hausdorff Distance (Kuehn 2015)

The Hausdorff Distance of two nonempty sets $V, W \subset \mathbf{R}^n$, for some $n \in \mathbf{N}$ is defined as

$$d_H(V, W) = \max\{\sup_{v \in V} \inf_{w \in W} \|v - w\|, \sup_{w \in W} \inf_{v \in V} \|v - w\|\}.$$

Now combining the above we can state Fenichel's Theorem.

Theorem 2.3 (Fenichel's Theorem (Desroches et al. 2012))

Suppose $M = M_0$ is a compact, normally hyperbolic submanifold (possibly with boundary) of the **critical manifold** S Equation ?? and that $f, g \in C^r$, $r < \infty$. Then for $\epsilon > 0$, sufficiently small, the following holds:

- (F1) There exists a locally invariant manifold M_ϵ , diffeomorphic to M_0 . Local invariance means that M_ϵ can have boundaries through which trajectories enter or leave.
- (F2) M_ϵ has a Hausdorff distance of $O(\epsilon)$ from M_0 .
- (F3) The flow on M_ϵ converges to the slow flow as $\epsilon \rightarrow 0$.
- (F4) M_ϵ is C^r -smooth.
- (F5) M_ϵ is normally hyperbolic and has the same stability properties with respect to the fast variables as M_0 (attracting, repelling or saddle type).
- (F6) M_ϵ is usually not unique. In regions that remain at a fixed distance from the boundary of M_ϵ , all manifolds satisfying (F1)-(F5) lie at a Hausdorff distance $O(e^{-K/\epsilon})$ from each other for some $K > 0$ with $K = O(1)$.
The normally hyperbolic manifold M_0 has associated local stable and unstable manifolds

$$W^s(M_0) = \cup_{p \in M_0} W^s(p) \quad \text{and} \quad W^u(M_0) = \cup_{p \in M_0} W^u(p),$$

where $W^s(p)$ and $W^u(p)$ are the local stable and unstable manifolds of p as a hyperbolic equilibrium of the layer equations, respectively. These manifolds also persist for $\epsilon > 0$, sufficiently small: there exist locally stable and unstable manifolds $W^s(M_\epsilon)$ and $W^u(M_\epsilon)$, respectively, for which conclusions (F1) - (F6) hold if we replace M_ϵ and M_0 by $W^s(M_\epsilon)$ and $W^s(M_0)$ (or similarly by $W^u(M_\epsilon)$ and $W^u(M_0)$).

Fenichel's Theorem establishes that the submanifold, M_0 , of the critical manifold, S_0 , persists as slow manifold M_ϵ as $\epsilon > 0$, given it is compact and normally hyperbolic. The theorem furthermore establishes that the stable and unstable manifolds persist as well as the individual fibres, namely $W^s(p)$ and $W^u(p)$, that are associated to each base point $p \in M_0$. Therefore, under the assumptions of the theorem, the flow of the Fast-Slow system remains $O(\epsilon)$ close to the flow of the system in the singular limit $\epsilon \rightarrow 0$.

The importance of this result lies in the fact that the behaviour of the full system can be analysed by looking at the system in the singular limit instead.

+++++also trajectories can be constructed and tested using fenichel... paper 1++++++

3 Singularities and Fold Points

One of the requirements of Fenichel's Theorem is normal hyperbolicity ([Kuehn 2015](#)). However, Fast-Slow systems can display singular points where normal hyperbolicity is no longer given and therefore the conclusions of Theorem 2.3 no longer hold at these singularities - where trajectories can jump between fast and slow flow. The singularities in the setting of Fast-Slow systems are points (x_0, y_0) on the critical manifold S_0 , for which the Jacobian (J at $\partial x(x_0, y_0, \lambda, 0)$) has one or more eigenvalue with zero real part. Comparing this with Definition 2.1 shows that this is a negation of normal hyperbolicity. The simplest of those singularities are called a fold point, which is defined as follows:

Definition 3.1. Fold Point

A fold point $(x_0, y_0) \in S_0$ is a point where the Jacobian $\frac{\partial f}{\partial x}(x_0, y_0, \lambda, 0)$ has only one eigenvalue with zero real part.

Moreover we say that the fold point is non-degenerate if it satisfies the non-degeneracy assumptions,

$$\begin{cases} \frac{\partial^2 f}{\partial x^2}(x_0, y_0, \lambda, 0) \neq 0, \\ \frac{\partial f}{\partial y}(x_0, y_0, \lambda, 0) \neq 0. \end{cases} \quad (8)$$

Furthermore, if (x_0, y_0) satisfies the transversality condition $g(x_0, y_0, \lambda, 0) \neq 0$, then it is called a generic fold point. For these generic folds there exists a theorem that states that the slow flow on S_ϵ near (x_0, y_0) has either positive or negative sign, implying that no equilibria of the slow flow are close to (x_0, y_0) . Therefore, for generic fold points no canards will be observed, which is a relevant observation for Section 5. First, we must find the fold points in the system.

3.1 Fold Points in the Van der Pol System

Considering the manifold $S = \{(x, y) : 0 = y - \frac{x^3}{3} + x^2 := f\}$, the Jacobian $\frac{\partial f}{\partial x}(x, y, 0) = 2x - x^2$, which has eigenvalues with zero real part at $x_0^{1,2} = 0, 2$ – together with the corresponding $y_0^{1,2}$ are singularities of the system. Further analysis has to be done below in order to conclude that they are generic fold points. The points of interest are $(x_0^1, y_0^1) = (0, 0)$ and $(x_0^2, y_0^2) = \left(2, \frac{4}{3}\right)$. By Definition 3.1, there is only one eigenvalue with zero real part at (x_0, y_0) . Evaluating the Jacobian at each of the points in turn shows:

$$\begin{cases} \frac{\partial f}{\partial x}(x_0^1, y_0^1, 0) = 0 \\ \frac{\partial f}{\partial x}(x_0^2, y_0^2, 0) = 0, \end{cases}$$

where each of the zeros are simple. Therefore (x_0^1, y_0^1) and (x_0^2, y_0^2) are fold points. These points are nondegenerate if the non-degeneracy assumptions (Equation 8) hold:

$$\begin{cases} \frac{\partial^2 f}{\partial x^2}(x_0^1, y_0^1, 0) = 2 - 2x_0^+ = 2 \neq 0 \\ \frac{\partial f}{\partial y}(x_0^1, y_0^1, 0) = -1 \neq 0, \end{cases}$$

and equivalently for the other fold point

$$\begin{cases} \frac{\partial^2 f}{\partial x^2}(x_0^2, y_0^2, 0) = -2x_0^2 = 4 \neq 0 \\ \frac{\partial f}{\partial y}(x_0^2, y_0^2, 0) = -1 \neq 0. \end{cases}$$

Therefore, the two fold points are non-degenerate. Furthermore, it can be checked if a fold point is generic. It then has to satisfy the transversality condition $g(x_0, y_0, 0) \neq 0$. The two fold points considered here are generic, since

$$\begin{aligned} g(x_0^1, y_0^1, 0) &= -1 \neq 0 \\ g(x_0^2, y_0^2, 0) &= 1 \neq 0. \end{aligned}$$

We know that normal hyperbolicity of the Van der Pol system breaks down at the fold points. Fenichel Theory can be applied for regions that are not in the neighbourhood of the fold points. However, a different approach has to be employed for the analysis of the dynamics around the folds. We need to use a new method called the Blow Up Method, which is discussed in Section 4.

Systems containing non-generic folds or other types of singularities can display different types of periodic orbits.

3.1.1 Extended System

The canonical system (Equation 4) is then extended to three dimensions by considering $\epsilon' = 0$.

$$\begin{aligned} x' &= -y + x^2 + h(x) \\ y' &= \epsilon(x - 1) \\ \epsilon' &= 0. \end{aligned} \tag{9}$$

Analysing the stability of the three dimensional system, three eigenvalues can be found by considering the Jacobian matrix, in the singular limit $\epsilon = 0$:

$$J = \begin{vmatrix} 2x - x^2 & -1 & 0 \\ 0 & 0 & 0 \\ 0 & 0 & 0 \end{vmatrix} \tag{10}$$

This is an upper triangular matrix and hence $(\lambda_1, \lambda_2, \lambda_3) = \text{tr}(J) = (2x - x^2, 0, 0)$. Therefore, at the fold points, where $x = 0$ or $x = 2$, $\lambda_i = 0$ for $i = 1, 2, 3$, there exists a zero eigenvalue on S . Note that at these points S is not normally hyperbolic. The critical manifold has to be divided as follows:

$$\begin{aligned} S^a &= \left\{ (x, y) : y = x^2 - \frac{x^3}{3}, x < 0 \right\} \cup \left\{ (x, y) : y = x^2 - \frac{x^3}{3}, x > 2 \right\} \\ S^r &= \left\{ (x, y) : y = x^2 - \frac{x^3}{3}, 0 < x < 2 \right\}, \end{aligned}$$

such that $S^a \cup S^r \cup \{0\} \cup \{2\} = S$. The manifolds S_0^a and S_0^r are normally hyperbolic everywhere and Theorem 2.3 (Fenichel's) can be applied in order to conclude the persistence of the manifold as slow manifolds S_ϵ^a and S_ϵ^r . At the points $x = 0$ and $x = 2$ the normal hyperbolicity is not given, since the eigenvalue associated to S is zero at these points.

In the analysis of the reduced system it became apparent that the fold points are singularities of the reduced flow on S_0 , and therefore the dynamics in the singular limit cannot be determined. Furthermore, Fenichel Theory does not apply at the folds because normal hyperbolicity breaks down at these points, as discussed above. Therefore, even if the dynamics around the folds in the singular limit were known, no conclusions could be drawn for the perturbed system with S_ϵ . Alternative methods have to be employed to describe the dynamics on the fold points in the singular limit and furthermore to be able to conclude the dynamics of the full system at the fold points from this analysis. The method considered for analysis is called the Blow-Up Method.

4 The Blow-Up Method

In order to apply the Blow-Up Method to the fold point at the origin, we focus on a neighbourhood U around the fold point $(0, 0)$. The neighbourhood U is small enough, such that $g(x, y, \epsilon) \neq 0$ in U , and we can define sections in U , as follows:

$$\begin{aligned} \Delta^{in} &= \{(x, \rho^2), x \in I\} \\ \Delta^{out} &= \{(\rho, y), y \in \mathbf{R}\}, \end{aligned}$$

where $I \subset \mathbf{R}$. Now Δ^{in} is transverse to S^a , while Δ^{out} is transverse to the fast flow. This enables us to monitor the incoming trajectories from the attracting branch of S and the trajectories leaving U in the direction of the

fast flow. Then a function $\pi : \Delta^{in} \rightarrow \Delta^{out}$ can be defined, called the transition map, which describes how the trajectories passing through Δ^{in} are mapped onto the outgoing flow in Δ^{out} . The following theorem describes the behaviour of the flow under π .

Theorem 4.1 (Krupa & Szmolyan 2001)

Under the assumptions made in this section, there exists $\epsilon_0 > 0$ such that the following assertions hold for $\epsilon \in (0, \epsilon_0]$:

1. The manifold S_ϵ^a passes through Δ^{out} at a point $(\rho, h(\epsilon))$, where $h(\epsilon) = O(\epsilon^{2/3})$.
2. The transition map π is a contraction with contraction rate $O(\epsilon^{-c/\epsilon})$, where c is a positive constant.

This means that the trajectories that enter U through Δ^{in} , will be funneled into a smaller section of Δ^{out} and therefore we are guaranteed to observe the trajectories that enter through Δ^{in} in Δ^{out} . Now we are in the position to describe the method of Blow-Up Transformations in the neighbourhood U .

4.1 Coordinate Transformation and Charts

We first need to transform the extended system (9) with respect to the time variable and the space variables. This coordinate transformation is called the Blow-Up Transformation because the degenerate fold point $(0, 0)$ is regarded as a sphere of radius $r = 0$. By rescaling the space variables with respect to different weights of r ,

$$x = \bar{r}\bar{x} \quad (11a)$$

$$y = \bar{r}^2\bar{y} \quad (11b)$$

$$\epsilon = \bar{r}^3\bar{\epsilon}, \quad (11c)$$

we find that we are able to carry out further analysis, as will follow. Instead of analysing the sphere in spherical polar coordinates, which might seem the most obvious choice of method, the rest of this analysis is done using charts, described below (see Needham (1998) for the construction of charts on a sphere). This method turns out to be a more natural choice for this problem and maximises computational efficiency. In terms of the blown

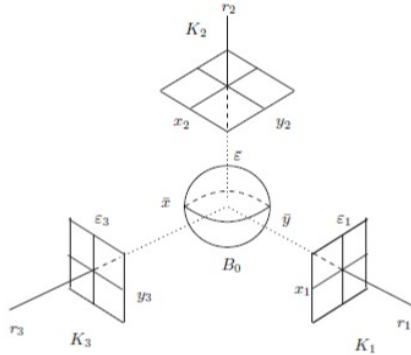


Figure 4: Three charts mapping different sections of our blow up (Krupa & Szmolyan 2001).

up fold point, a sphere denoted by B , charts are projections of regions of B onto a two dimensional plane. We introduce three charts K_1, K_2 , and K_3 . Chart K_2 is the two dimensional projection covering the upper half plane of B . However, as points on the equator of B are approached on K_1 , the point tends to infinity. These regions however, are of immense interest, since they are points of incoming and outgoing trajectories. As a consequence, charts K_1 and K_3 are introduced, covering the regions of interest on the equator of the fold point. The charts

are defined by setting each of the variables of the extended system to 1 in turn, giving $\bar{y} = 1$, $\bar{\epsilon} = 1$, $\bar{x} = 1$. Substituting these into Equations (11a), (11b) and (11c) respectively gives,

$$x = r_1 x_1, \quad y = r_1^2, \quad \epsilon = r_1^3 \epsilon_1, \quad (12a)$$

$$x = r_2 x_2, \quad y = r_2^2 y_2, \quad \epsilon = r_2^3 \quad (12b)$$

$$x = r_3, \quad y = r_3^2 y_3, \quad \epsilon = r_3^3 \epsilon_3 \quad (12c)$$

where $(x_i, r_i, \epsilon_i) \in \mathbf{R}^3$ for $i = 1, 2, 3$, and the equations correspond to the charts in numerical order (Krupa & Szmolyan 2001). With this setup, we can consider the individual charts in turn, analyse the dynamics on the individual charts, and then join the gathered information into a global view on the dynamics in U . We start with K_2 , because it holds the most information and the flow is the analysed more readily than in the other two charts. The remaining question is how the transition between the three charts and the connection to the global dynamics is made after finishing the individual analysis. This is done via a coordinate change, derived by using Equations 12 and 11, and the results are summarised in the following Lemma:

Lemma 4.2

Let κ_{12} denote the change of coordinates from K_1 to K_2 . Then κ_{12} is given by

$$x_2 = x_1 \epsilon_1^{-1/3}, \quad y_2 = \epsilon_1^{-2/3}, \quad r_2 = r_1 \epsilon_1^{1/3},$$

for $\epsilon_1 > 0$, and κ_{12}^{-1} is given by

$$x_1 = x_2 y_2^{-1/2}, \quad r_1 = r_2 y_2^{1/2}, \quad \epsilon_1 = y_2^{-3/2},$$

for $y_2 > 0$. Let κ_{23} denote the change of coordinates from K_2 to K_3 . Then κ_{23} is given by

$$r_3 = r_2 x_2, \quad y_3 = y_2 x_2^{-2}, \quad \epsilon_3 = x_2^{-3},$$

for $x_2 > 0$, and κ_{23}^{-1} is given by

$$x_2 = \epsilon_3^{-1/3}, \quad y_2 = y_3 \epsilon_3^{-2/3}, \quad r_2 = r_3 \epsilon_3^{1/3},$$

for $\epsilon_3 > 0$.

Furthermore, transition maps $\Pi_i, i \in 1, 2, 3$ are defined in each section, describing how the trajectories coming in and out of each chart. These are combined in the final part of this section to give the proof of Theorem 4.1, and to relate the results of the blow up method back to the original transition map π .

4.2 Dynamics in K_2

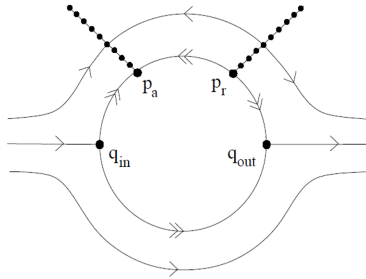


Figure 5: Phase portrait for chart 2 (Krupa & Szmolyan 2001).

To be able to consider chart K_2 , the transformation presented in Equation 12b is applied to the extended system (9). Furthermore, a time rescaling ($t_2 = r_2 t$) is applied to desingularise the system. This results in:

$$\begin{aligned} \frac{d}{dt}(r_2 x_2) &= r_2^2 \frac{dx_2}{dt} = -y_2 + x_2^2 - \frac{x_2^3 r_2}{3}, \\ r_2^3 y'_2 &= r_2^3 (-1 + r_2 x), \\ r'_2 &= 0, \end{aligned} \tag{13}$$

noting that $\frac{dr}{dt_2} = \frac{dt}{dt_2} \frac{dr}{dt} = \frac{1}{r_2} \frac{dr_2}{dt}$. Now dividing through by r_2^2 and r_2^3 respectively for each equation and grouping $O(r_2)$ terms we get,

$$\begin{aligned} x'_2 &= x_2^2 - y_2 + O(r_2), \\ y'_2 &= -1 + O(r_2), \\ r'_2 &= 0. \end{aligned} \tag{14}$$

Then, considering $r_2 = 0$ and neglecting the $O(r_2)$ terms results in,

$$\begin{aligned} x'_2 &= x_2^2 - y_2, \\ y'_2 &= -1, \end{aligned} \tag{15}$$

which are the well known Riccati equations- see Mishchenko (2012). Some known results about the Riccati equations can be summarised as follows:

Proposition 4.3 (Krupa & Szmolyan 2001)

The Riccati equation (15) has the following properties:

1. Every orbit has a horizontal asymptote $y = y_r$, where y_r depends on the orbit such that $x \rightarrow \infty$ as y approaches y_r from above.
2. There exists a unique orbit γ_2 , which can be parameterized as $(x, s(x))$, $x \in \mathbf{R}$ and is asymptotic to the left branch of the parabola $x^2 - y = 0$, for $x \rightarrow -\infty$. The orbit γ_2 has a horizontal asymptote $y = -\Omega_0 < 0$, such that $x \rightarrow \infty$ as y approaches $-\Omega_0$ from above.
3. The function $s(x)$ has the asymptotic expansions

$$\begin{aligned} s(x) &= x^2 + \frac{1}{2x} + O\left(\frac{1}{x^4}\right), x \rightarrow -\infty, \\ s(x) &= -\Omega_0 + \frac{1}{x} + O\left(\frac{1}{x^3}\right), x \rightarrow \infty. \end{aligned}$$

4. All orbits to the right of γ_2 are backward asymptotic to the right branch of the parabola $x^2 - y = 0$.
5. All orbits to the left of γ_2 have a horizontal asymptote $y = y_l > y_r$, where y_l depends on the orbit, such that $x \rightarrow -\infty$ as y approaches y_l from below.

The solutions to the Riccati equations, described in Proposition 4.3, are displayed in Figure. Note that the equation $x^2 - y = 0$ is locally the critical manifold S close to the fold point. The orbit γ_2 , corresponds to the global trajectory γ , of the full system, which is the candidate trajectory connecting the slow flow on S^a entering U through p_a to the fast fibres, exiting U through q_{out} - described by Figure 6.

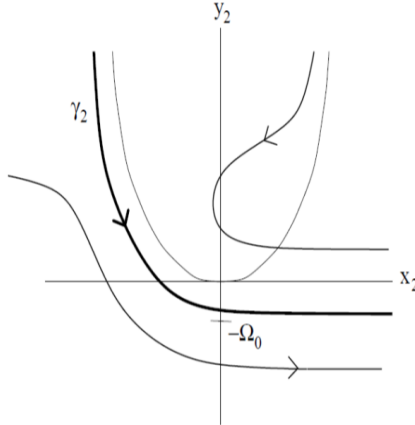


Figure 6: Riccati solution for chart 2 ([Krupa & Szmolyan 2001](#)).

This leads to the conclusion that if we can connect γ_2 to p_a through K_1 and to q_{out} through K_3 , the global γ can be constructed using Lemma 4.2. This motivates the analysis of K_1 and K_3 . In order to connect the dynamics on K_2 to that on the other charts, we need to define local inflow and outflow sections, similar to Δ^{in} and Δ^{out} in the full system. Then we can follow trajectories that get mapped by Π_2 , again analogous to π in the full system, from a section Σ_2^{in} to Σ_2^{out} . The sections are defined as follows. For $\delta > 0$, we have:

$$\begin{aligned}\Sigma_2^{in} &= \{(x_2, y_2, r_2) : y_2 = \delta^{-2/3}\}, \\ \Sigma_2^{out} &= \{(x_2, y_2, r_2) : x_2 = \delta^{-1/3}\}.\end{aligned}$$

Then the transition map Π_2 can be defined and the results are summarised as follows:

Proposition 4.4 ([Krupa & Szmolyan 2001](#))

The transition map Π_2 has the following properties:

1.

$$\Pi_2(q_0) = (\delta^{-1/3}, -\Omega_0 + \delta^{1/3} + O(\delta), 0)$$

2. A neighbourhood of q_0 is mapped diffeomorphically onto a neighbourhood of $\Pi_2(q_0)$.

This is sufficient information to now consider the dynamics on K_1 .

4.3 Dynamics in K_1

The coordinate transformation (12a) is applied to the extended system (9),

$$\begin{aligned}\frac{d(r_1 x_1)}{dt_1} \frac{dt_1}{dt} &= -r_1^2 + r_1^2 x_1^2 - \frac{1}{3} r_1^3 x_1^3, \\ \frac{dr_1^2}{dt_1} \frac{dt_1}{dt} &= 2r_1^2 r_1' = r_1^3 \epsilon_1 (-1 + r_1 x_1), \\ \frac{d(r_1^3 \epsilon_1)}{dt_1} \frac{dt_1}{dt} &= (3r_1^2 \epsilon_1 + r_1^3 \epsilon_1') r_1 = 0.\end{aligned}$$

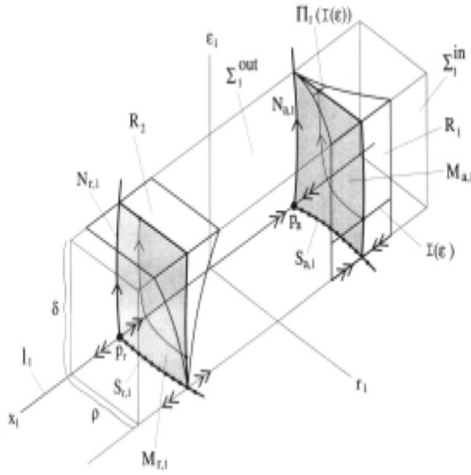
Dividing through by $\frac{dt_1}{dt} = r_1$ and replacing the expressions for ϵ_1' and r_1' with their expressions in terms of the variables, results in the full system in terms of K_1 . Note that the equation for ϵ' is found by rearranging the third equation above.

$$\begin{aligned}x_1' &= -1 + x^2 + \frac{1}{2} x_1 \epsilon_1 + \left(-\frac{1}{2} \epsilon_1 x_1^2 r_1 - \frac{1}{3} x_1^3 \right) \\ r_1' &= \frac{1}{2} r_1 \epsilon_1 (-1 + r_1 x_1) \\ \epsilon_1' &= \frac{3}{2} \epsilon_1^2 (1 - r_1 x_1),\end{aligned}$$

and grouping terms in r_1 results in the standard form:

$$\begin{aligned}x_1' &= -1 + x^2 + \frac{1}{2} x_1 \epsilon_1 + O(r_1) \\ r_1' &= \frac{1}{2} r_1 \epsilon_1 (-1 + O(r_1)) \\ \epsilon_1' &= \frac{3}{2} \epsilon_1^2 (1 - O(r_1)).\end{aligned}\tag{16}$$

The system (16) has two invariant planes, that are somewhat equivalent to the notion of a nullcline. This tell us that the rate of change for our confidantes, r_1 and ϵ_1 is constant for $r_1 = 0$ and $\epsilon_1 = 0$. If we substitute $r_1 = 0$ or $\epsilon_1 = 0$ into (16), the r_1 or ϵ_1 equation respectively, are both zero, and there is only a two dimensional system left to consider. These two subspaces of (16) will be analysed below. Furthermore, the subspace where $r_1 = 0$ and $\epsilon_1 = 0$, is one dimensional, an invariant line, where the subspaces $r_1 = 0$ and $\epsilon_1 = 0$ cross. The following analysis is displayed in Figure 7, illustrating the dynamics on K_1 .


 Figure 7: Dynamics in chart 1 ([Krupa & Szmolyan 2001](#))

The invariant line, satisfying $r_1 = 0$ and $\epsilon_1 = 0$ is given by $l_1 = -1 + x^2$. From this it is easily deduced that the two equilibrium points are where $l_1 = 0$, which is at $x = \pm 1$. Therefore, the points p_a and p_r are defined as $p_a = (-1, 0, 0)$ and $p_r = (1, 0, 0)$. The flow on l_1 is attracted to p^a and repelled by p^r , which is easily observed from the form l_1 takes or from a formal stability analysis of the one dimensional system. The eigenvalues of l_1 are found by considering $l'_1 - \lambda = 2x - \lambda = 0$ which gives that $\lambda = \pm 2$ at the respective equilibria. Then we expect the behaviour of the flow on the two invariant planes to be influenced by the two equilibria and the dynamics on l_1 . Consider the plane $\epsilon_1 = 0$. The system (Equation 16) becomes

$$\begin{aligned} x'_1 &= -1 + x_1^2 - \left(\frac{1}{3} r_1 x_1^3 \right) \\ r'_1 &= 0. \end{aligned} \tag{17}$$

This system has equilibria at $x = \pm 1$, for $r_1 = 0$, as before, however, for each constant value of r_1 , we get a different equilibrium of the system (17). This forms a curve of equilibria, which can be recognised as S_1^a connected to p_a and S_1^r connected to p_r , of the critical manifold, transformed into K_1 - this follows from the Implicit Function Theorem, see Figure 5. The additional eigenvalue, corresponding to the r_1 equation, is $\lambda = 0$. However, at each of the equilibria of this system, and specifically at p_a and p_r we have normal hyperbolicity, due to the coordinate transformation in K_1 . Next we consider the dynamics on the invariant plane $r_1 = 0$. The system (Equation 16) becomes:

$$\begin{aligned} x'_1 &= -1 + x_1^2 + \frac{1}{2} x_1 \epsilon_1 \\ \epsilon'_1 &= \frac{3}{2} \epsilon_1^2. \end{aligned} \tag{18}$$

Again, $x = \pm 1$ are equilibria of the system, and an additional zero eigenvalue is gained due to the ϵ equation. It can be concluded that one dimensional centre manifolds exist, called $N_{a,1}$ and $N_{r,1}$, that are invariant, but not manifolds of equilibria like S^a and S^r in the $\epsilon = 0$ plane. The dynamics on these manifolds are determined mainly by the value of ϵ , since the change in the ϵ direction is much stronger than the change in the x direction. Therefore, on $N_{a,1}$ and $N_{r,1}$ the flow moves in the ϵ direction with increasing epsilon. In order to draw conclusions on the persistence of the dynamics in the full system, sections in the space are defined to monitor incoming and outgoing

trajectories. Firstly, let the region considered be such that $D_1 := \{(x_1, y_1, \epsilon_1) : x_1 \in \mathbf{R}, 0 \leq r_1 \leq \rho, 0 \leq \epsilon_1 \leq \delta\}$. Then the relevant sections for the candidate trajectory γ are

$$\begin{aligned}\Sigma_1^{in} &:= \{(x_1, r_1, \epsilon_1) \in D_1 : r_1 = \rho\}, \\ \Sigma_1^{out} &:= \{(x_1, r_1, \epsilon_1) \in D_1 : \epsilon_1 = \delta\}.\end{aligned}$$

Note that $\Sigma_1^{in} = \Delta^{in}$ and $\Sigma_1^{out} = \Sigma_2^{in}$. The aim is to find the connection between p_a and γ_2 in K_2 . In order to establish this connection, the trajectory γ_2 has to be mapped onto K_1 using Lemma 4.2. Recall from Section 4.2 that the form of the candidate trajectory is of the form $(x_2, s(x_2))$. Therefore, the trajectory γ_1 satisfies:

$$(x_1, 0, \epsilon_1) = \left(x_2 \left(x_2^2 + \frac{1}{2x_2} + O\left(\frac{1}{x_2^4}\right) \right)^{-1/2}, 0, \left(x_2^2 + \frac{1}{2x_2} + O\left(\frac{1}{x_2^4}\right) \right)^{-3/2} \right).$$

Note that $s(x_2)$ as $x_2 \rightarrow -\infty$ is employed, since we consider the left continuation of γ_2 . Furthermore, as is intuitively clear from Figure 6, and can be shown by analysing the form of γ_1 , the trajectory γ_1 converges to p_a in backward time, which is exactly as expected. This establishes the link between the slow flow on S^a and the flow on K_2 , if we consider the following proposition, which sums up the findings in K_1 and employs center manifold theory in order to establish persistence in the full system.

Proposition 4.5 (Krupa & Szmolyan 2001)

For ρ, δ sufficiently small the following assertions hold for the system 16:

1. There exists an attracting two-dimensional C^k -center manifold $M_{a,1}$ at p_a which contains the line of equilibria S_1^a and the center manifold $N_{a,1}$. In D_1 the manifold $M_{a,1}$ is given as a graph $x_1 = h_a(r_1, \epsilon_1)$. The branch of $N_{a,1}$ in $r_1 = 0, \epsilon_1 > 0$ is unique.
2. There exists a repelling two-dimensional C^k -center manifold $M_{r,1}$ at p_r which contains the line of equilibria S_1^r and the center manifold $N_{r,1}$. In D_1 the manifold $M_{r,1}$ is given as a graph $x_1 = h_r(r_1, \epsilon_1)$. The branch of $N_{r,1}$ in $r_1 = 0, \epsilon_1 > 0$ is not unique.
3. There exists a stable invariant foliation F^s which base $M_{a,1}$ and one-dimensional fibres. For any $c > -2$ there exists a choice of positive ρ and δ such that the contraction along F^s during a time interval $[0, T]$ is stronger than e^{cT} .
4. There exists an unstable invariant foliation F^u which base $M_{r,1}$ and one-dimensional fibres. For any $c > -2$ there exists a choice of positive ρ and δ such that the expansion along F^u during a time interval $[0, T]$ is stronger than e^{cT} .
5. The unique branch $N_{a,1}$ in $r_1 = 0, \epsilon_1 > 0$ is equal to $\gamma_1 := \kappa_{12}^{-1}(\gamma_2)$ wherever $\kappa_{12}^{-1}(\gamma_2)$ is defined, i.e. along the part of γ_2 corresponding to $y_2 > 0$.

In order to find the lower bound on the contraction rate along F^s , the transition time T has to be found, i.e. the time the trajectory takes to travel from a point $p = (x_1, \rho, \epsilon_1) \in \Sigma_1^{in}$ to a point in $\Pi_1(p) = (x_1, r_1, \delta) \in \Sigma_1^{out}$. This is done by integrating the ϵ equation of system (16), which is a separable ODE with respect to t_1 . This then results in

$$T = \frac{2}{3} \left(\frac{1}{\epsilon_1} - \frac{1}{\delta} \right) (1 + O(\rho)),$$

where $r_1 = \rho \in p$. Therefore, a transition map $\Pi_1 : \Sigma_1^{in} \rightarrow \Sigma_1^{out}$ can be defined for small enough parameter values of ρ, δ, β_1 . We are interested specifically in the transition around the center manifolds $M_{a,1}$ and $M_{r,1}$. The

following subsections of Σ_1^{in} and Σ_1^{out} can be defined. Let $R_1 = \{(x_1, \rho, \epsilon_1) : |1 + x_1| \leq \beta_1\}$, a rectangle in the intersection of the manifolds $M_{a,1}$ and Σ_1^{in} , and $R_2 = \{(x_1, r_1, \delta) : |1 - x_1| \leq \beta_1\}$, a rectangle in the intersection of the manifolds $M_{r,1}$ and Σ_1^{out} , with $\beta_1 > 0$ sufficiently small. Furthermore, we can define line segments in these rectangles as $I_a(\bar{\epsilon}) \subset R_1$ and $I_r(\bar{r}) \subset R_2$, where $0 \leq \bar{\epsilon} \leq \delta$ and $0 \leq \bar{r} \leq \rho$. Then for any $\bar{\epsilon}$, Π_1 maps the trajectory on a smaller region $\Pi_1 I_a(\bar{\epsilon}) \in \Sigma_1^{out}$. This is called a contraction of the trajectories. Considering Theorem 4.1, which states the dependence of the contraction rate on ϵ , the bounds on the contraction rate can be related to ϵ , the parameter of the original system. Then using the K_1 rescaling of $\epsilon = \epsilon_1 r_1^3$, see Equation 12a, the contraction rate for $\Pi_1|I_r(\bar{r})$ is found by replacing ϵ_1 by $\frac{\delta r_1^3}{\rho^3}$. Visual understanding of this analysis can be gained by considering Figure 7. The following proposition summarises the findings for Π_1 :

Proposition 4.6 (Krupa & Szmolyan 2001)

For ρ, δ and β_1 sufficiently small, the transition map $\Pi_1 : \Sigma_1^{in} \rightarrow \Sigma_1^{out}$ defined by the flow of system 16 has the following properties:

1. $\Pi_1(R_1)$ is a wedge-like region in Σ_1^{out} . $\Pi_1^{-1}(R_2)$ is a wedge-like region in Σ_1^{in} .
2. More precisely, for fixed $c < 2$, there exists a constant K depending on the constants c, ρ, δ and β_1 such that:
 - (a) for $\bar{\epsilon} \in (0, \delta]$ the map $\Pi_1|I_a(\bar{\epsilon})$ is a contraction with contraction rate bounded by $Ke^{-\frac{2c}{3}(\frac{1}{\bar{\epsilon}} - \frac{1}{\delta})}$.
 - (b) for $\bar{r} \in (0, \rho]$ the map $\Pi_1|I_r(\bar{r})$ is a contraction with cocontraction rate bounded by $Ke^{-\frac{2c}{3}(\frac{\rho^3}{r_1^3 \delta} - \frac{1}{\delta})}$.

4.4 Dynamics in K_3

The final chart to study the behaviour of is K_3 . This chart covers the trajectory as it leaves the fold point at q_{out} . The other charts could not do this as q_{out} is close to infinity in both K_1 and K_3 (cf. Figure 4). Similarly to K_1 and K_2 , the system can be analysed using the blow-up transformation (12c).

$$\frac{dr_3}{dt_3} = r_3 F(r_3, y_3, \epsilon_3) \quad (19a)$$

$$\frac{dy_3}{dt_3} = \epsilon_3(r_3 - 1) - 2y_3 F(r_3, y_3, \epsilon_3) \quad (19b)$$

$$\frac{d\epsilon_3}{dt_3} = -3\epsilon_3 F(r_3, y_3, \epsilon_3) \quad (19c)$$

where $F(r_3, y_3, \epsilon_3) = (1 - y_3 - \frac{r_3}{3})$. Note that as ϵ_3 and r_3 appear as a factor in their respective derivatives, the planes $\epsilon_3 = 0$ and $r_3 = 0$ are invariant and, by extension, so is the y_3 axis. The aim is to continue the special trajectory found in the other two charts and to find the transition map in and out of this chart. We will then be able to construct a phase portrait for the whole space by combining the dynamics in each chart. Linearising the system about $(0, 0, 0) = q_{out}$ gives

$$\begin{pmatrix} \dot{r}_3 \\ \dot{y}_3 \\ \dot{\epsilon}_3 \end{pmatrix} = \begin{pmatrix} 1 & 0 & 0 \\ 0 & -2 & -1 \\ 0 & 0 & -3 \end{pmatrix} \begin{pmatrix} r_3 \\ y_3 \\ \epsilon_3 \end{pmatrix}$$

As the matrix is upper triangular, its eigenvalues are trivially $\{1, -2, -3\}$ with corresponding eigenvectors $\{(1, 0, 0), (0, 1, 0), (0, 1, 1)\}$. This presents an issue as there is additive resonance i.e. $\lambda_2 - (\lambda_1 + \lambda_3) = 0$. This

means the Poincaré-Dulac theorem does not hold and the vector field is not linearisable, there is no smooth transformation between the nonlinear and linear flow. Despite this, progress can still be made as the form of the equations allow a near identity transformation and yields the lowest order approximation to the flow. The special orbit, γ_2 , can be mapped into this chart using the change of coordinates κ_{23} of Equation 4.2.

$$\gamma_3 = \kappa_{23}(\gamma_2)$$

In fact, γ_3 lies in the plane $r_3 = 0$ and converges to q_{out} as $\epsilon \rightarrow 0$. To find the flow in a neighbourhood of q_{out} we use sections similar to those introduced in K_2 .

$$\begin{aligned}\Sigma_3^{in} &= \{(r_3, y_3, \epsilon_3) : r_3 \in [0, \rho], y_3 \in [-\beta_3, \beta_3], \epsilon_3 = \delta\}, \\ \Sigma_3^{out} &= \{(r_3, y_3, \epsilon_3) : r_3 = \rho, y_3 \in [-\beta_3, \beta_3], \epsilon_3 \in [0, \delta]\}\end{aligned}$$

We now wish to find the transition map Π_3 between these two charts. That is, given that the trajectory enters somewhere in Σ_3^{in} , how will it behave until it reaches Σ_3^{out} ? To do this, the system 19 will be studied after some simplification. The system is in fact equivalent to the Riccati equation. Observe that $F(r_3, y_3, \epsilon_3)|_{q_{out}} = 1 - y_3 + O(r_3)|_{q_{out}} \approx 1$. Thus dividing (19) through by F yields

$$\dot{r}_3 = r_3 \tag{20a}$$

$$\dot{y}_3 = -2y_3 - \frac{\epsilon_3}{1 - y_3} + r_3\epsilon_3 G(r_3, y_3, \epsilon_3) \tag{20b}$$

$$\dot{\epsilon}_3 = -3\epsilon_3 \tag{20c}$$

In the invariant plane $r_3 = 0$, the system becomes the Riccati equation (cf. (15)) transformed into the chart K_3 and with a rescaling of time.

$$\begin{aligned}y'_3 &= -2y_3 - \frac{\epsilon_3}{1 - y_3} \\ \epsilon'_3 &= -3\epsilon_3\end{aligned}$$

This system has eigenvalues $\{-2, -3\}$ and the issue of additive resonance has been avoided so we are able to linearise the system using a near-identity transformation. This transformation allows the elimination of awkward higher order terms (in this case, $\frac{1}{1-y_3}$). Let

$$y_3 = \psi(\tilde{y}_3, \epsilon_3) = \tilde{y}_3 + O(\tilde{y}_3\epsilon_3).$$

Let $\tilde{\psi}$ denote the inverse transformation and both be C^k functions. The system (20) can now be linearised and the following proposition gives the transition map.

Proposition 4.7 (Krupa & Szmolyan 2001)

The transition map Π_3 for the transformed K_3 system (19) is

$$\Pi_s(r_3, y_3, \delta) = \begin{pmatrix} \rho \\ \Pi_{32}(r_3, y_3, \delta) \\ \left(\frac{r_3}{\rho}\right)^3 \delta \end{pmatrix}$$

where

$$\Pi_{32}(r_3, y_3, \delta) = (\bar{\psi}(y_3, \delta) - \delta) \left(\frac{r_3}{\rho}\right)^2 + O(r_3^3 \ln r_3)$$

Proof. We will use the near-identity transformation to find the passage time T and thus the values of r_3, y_3, ϵ_3 at this time. For brevity, the subscripts will be omitted for the remainder of this proof. Under the near-identity transformation, system (20) becomes

$$\dot{r} = r, \quad (21a)$$

$$\dot{\tilde{y}} = -2\tilde{y} + \epsilon + r\epsilon H(r, \tilde{y}, \epsilon) \quad (21b)$$

$$\dot{\epsilon} = -3\epsilon \quad (21c)$$

Let the subscript i denote the value of a variable at its entry into the chart, and likewise o for out. Then $(r_i, y_i, \epsilon_i) \in \Sigma^{in}$, and $(r_o, y_o, \epsilon_o) \in \Sigma^{out}$. Thus

$$\begin{aligned} r(0) &= r_i & r(T) &= r_o = \rho \\ y(0) &= y_i & y(T) &= y_o \\ \epsilon(0) &= \epsilon_i = \delta & \epsilon(T) &= \epsilon_o \end{aligned}$$

We wish to construct an equation for the out variables $(T, \tilde{y}_o, \epsilon_o)$ in terms of the in variables (r_i, \tilde{y}_i) , that is the transition map. The r and ϵ equations are easily solved:

$$r = r_i e^t \quad \epsilon = \delta e^{-3t} \quad (22)$$

Then using $r(T) = \rho$,

$$r(T) = \rho = r_i e^{-t} \implies T = \ln\left(\frac{\rho}{r_i}\right).$$

For the equation in y , a little more work is required. We introduce a new coordinate z as follows, $\tilde{y} = e^{-2t}(\tilde{y}_i - \delta + z) + \delta e^{-3t}$. Upon first sight, this seems unlikely to be of any use. However, it turns out that this transformation is ideal as it allows many terms to be removed. First rearrange for z and differentiate with respect to t .

$$\begin{aligned} z &= e^{2t}(\tilde{y} - \delta e^{-3t}) - \tilde{y}_i + \delta \\ \frac{dz}{dt} &= 2e^{2t}\tilde{y} + e^{2t}\dot{\tilde{y}} + \delta e^{-t} \end{aligned}$$

Substitute $\dot{\tilde{y}}$ from Equation (21b) and cancel terms.

$$\begin{aligned} &= e^{2t}(-\epsilon + r\epsilon H(r, \tilde{y}, \epsilon)) + \delta e^{-t} \\ &= -\epsilon e^{2t} + e^{2t}r\epsilon H(r, \tilde{y}, \epsilon) + \delta e^{-t} \\ &= e^{2t}r\epsilon H(r, \tilde{y}, \epsilon) \end{aligned}$$

This final equality follows from the explicit solutions in r and ϵ above. These equations also show that $r\epsilon e^{2t} = r_i \delta e^{-2t} e^{2t}$. Finally,

$$\dot{z} = r_i H^z(r_i, \tilde{y}_i, t)$$

where H^z is the same as H but under the transformation from z , i.e. $H^z(r_i, \tilde{y}_i, t) = \delta H(r_i e^t, e^{-2t}(\tilde{y}_i - \delta + z) + \delta e^{-3t}, \delta e^{-3t})$. This has not affected the expression for the passage time T . ++Uniform boundedness of H implies?++ Hence $z(T) = r_i O(T) = O(r_i \ln(\frac{\rho}{r_i}))$ Using the initial definition of z , we recover an expression for $\tilde{y}(T)$.

$$\begin{aligned} \tilde{y}(T) &= e^{-2T} \left(\tilde{y}_i - \delta + O\left(r_i \ln\left(\frac{\rho}{r_i}\right)\right) \right) + \delta e^{-3T} \\ &= (\tilde{y}_i - \delta)e^{-2 \ln \frac{\rho}{r_i}} + e^{-2 \ln \frac{\rho}{r_i}} O\left(r_i \ln \frac{\rho}{r_i}\right) + \delta \frac{r_i^3}{\rho^3} \\ &= (\tilde{y}_i - \delta) \frac{r_i^2}{\rho^2} + O\left(\frac{r_i^3}{\rho^2} \ln \frac{\rho}{r_i}\right) \end{aligned}$$

We now have an expression for each of the out variables in terms of the initial conditions, albeit under a near-identity transformation. All that remains is to undo this transformation using the inverse map $\tilde{\psi}$.

+++Undo transformation, explain r and ϵ coordinates in prop. ThenDONE!+++ ■

4.5 The Full Solution

The analysis of the three charts, discussed in the Sections 4.2-4.4, provided a description of the dynamics on each of the charts, as well as theory to conclude the persistence of the dynamics in the full system. The special trajectory γ has been traced through all charts and in chart 1 it has been linked to the slow flow of S^a , while in chart 3 the connection to the fast flow has been made. Therefore, the fold point is indeed a jump point, or transition point, which connects the slow and fast dynamic. These transition points can also be seen in the case of singular canards, which are treated in the following section. The remaining issue is the transition of this special trajectory through the charts in order to have a solution of the full system. This is equivalent to finding the transition map π from Theorem 4.1. Let $\Pi : \Sigma_1^{in} \rightarrow \Sigma_3^{out}$ be the full transition map of the Blow-Up Transformation. Then it satisfies

$$\Pi := \Pi_3 \circ \kappa_{23} \circ \Pi_2 \circ \kappa_{12} \circ \Pi_1,$$

where κ is the change of coordinates defined in Lemma 4.2 and Π_1, Π_2, Π_3 are the transition maps in each chart. Finally, reversing the blow up transformation gives the full transition map π and therefore there exists a trajectory γ in the blow down vector field connecting slow and fast flow. With this analysis at hand we are now able to describe the full dynamics of the Van der Pol system when $\epsilon > 0$ by analysing the singular limit $\epsilon \rightarrow 0$. The full result is visualised in Figure ??.



(a) The flow on the Van der Pol for a small ϵ .

(b) The flow on the Van der Pol for a larger ϵ .

Figure 8: Flow on the Van der Pol system.

5 Canard in Two Dimensions

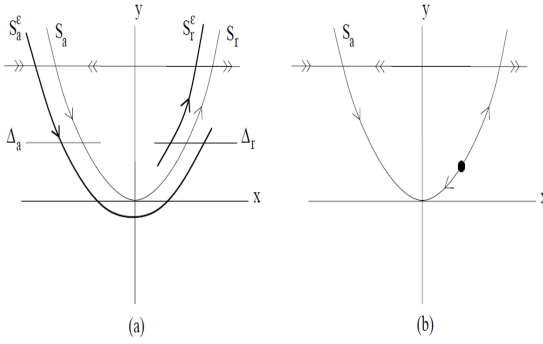


Figure 9: The reduced flow where a) $\lambda = 0$ and b) $\lambda > 0$.

Considering the Van der Pol System as before:

$$\begin{aligned} x' &= -y + x^2 - \frac{x^3}{3}, \\ y' &= \epsilon(x - 1), \end{aligned} \tag{??}$$

we notice that the equilibrium of the system depends on the two nullclines $x' = 0$ and $y' = 0$. These are in the shape of a cubic function and in the shape of a vertical line at $x = 1$. The idea in this section is to replace the nullcline $x = 1$ by $x = \lambda$. This can be seen as shifting the equilibrium of the system along the critical manifold S by varying the parameter λ . This gives rise to a generalised Van der Pol system:

$$\begin{aligned} x' &= -y + x^2 - \frac{x^3}{3}, \\ y' &= \epsilon(x - \lambda). \end{aligned} \tag{23}$$

In this section, the dynamics in system 26 is analysed. In order to do so, we need the definition of a canard.

Definition 5.1. *Canard*[Kuehn 2015] *A trajectory of a fast-slow system is called a canard if it stays within $O(\epsilon)$ close to the repelling branch S^r of the slow manifold S , for some time of $O(1)$ on the slow time scale $\tau = \epsilon t$.*

Furthermore, the following definition turns out to be useful as well:

Definition 5.2. Maximal Canard[Kuehn 2015] *The trajectory passing through the intersection of S^a and S^r is called a maximal canard.*

Definition 5.3. Singular Canard

The intuition of the canard problem close to a fold point is given in Figure 9. Equivalently to the analysis of the fold point in Section ??, some nondegeneracy conditions are defined. These are, as before, applied at the fold point $(0,0)$. Note that in contrast to the nondegeneracy conditions in (8), the transversality condition $g(0,0,0) \neq 0$ is not satisfied. Therefore higher order conditions on g have to be employed, in particular these are nonzero derivatives of g with respect to x and λ . The fact that $g_x(0,0,0) \neq 0$ guarantees the existence of transversal intersection of the two nullclines, which is crucial in order to conclude persistence of the dynamics later on (?). The nondegeneracy and transversality conditions for the canard case are (Krupa & Szmolyan 2001),

$$f(0,0,0,0) = 0, \quad \frac{\partial}{\partial x} f(0,0,0,0) = 0, \quad g(0,0,0,0) = 0, \tag{24}$$

$$\begin{aligned} \frac{\partial^2}{\partial x^2} f(0, 0, 0, 0) &\neq 0, \quad \frac{\partial}{\partial y} f(0, 0, 0, 0) \neq 0, \\ \frac{\partial}{\partial x} g(0, 0, 0, 0) &\neq 0, \quad \frac{\partial}{\partial \lambda} g(0, 0, 0, 0) \neq 0. \end{aligned} \tag{25}$$

Now that these conditions have been defined we can consider, equivalent to the argument in Section 3.1.1, the extended Van der Pol system,

$$\begin{aligned} x' &= -y + x^2 - \frac{x^3}{3}, \\ y' &= \epsilon(x - \lambda), \\ \epsilon' &= 0, \\ \lambda' &= 0, \end{aligned} \tag{26}$$

where the change in ϵ and λ are constant. Now, for the remainder of the section, we apply the method of Krupa & Szmolyan (2001) to the Van der Pol System. The canonical form for the Canard System is:

$$\begin{aligned} x' &= -yh_1(x, y, \epsilon, \lambda) + x^2h_2(x, y, \epsilon, \lambda) + \epsilon h_3(x, y, \lambda, \epsilon) \\ &= -y + x^2 \left(1 - \frac{x}{3}\right), \\ y' &= \epsilon(xh_4(x, y, \epsilon, \lambda) - \lambda h_5(x, y, \epsilon, \lambda) + yh_6(x, y, \lambda, \epsilon)) \\ &= \epsilon(x - \lambda). \end{aligned} \tag{27}$$

It follows that $h_1 = 1$, $h_2 = 1 - \frac{x}{3}$, $h_3 = 0$, $h_4 = 1$, $h_5 = 1$ and $h_6 = 0$. It is possible to find a $\lambda > 0$, for which an equilibrium on the repelling branch S_r exists for the reduced dynamics. The following definition can be made in order to simplify the following computations:

$$\begin{aligned} a_1 &= \frac{\partial}{\partial x} h_3(0, 0, 0, 0) = 0 & a_2 &= \frac{\partial}{\partial x} h_1(0, 0, 0, 0) = 0 & a_3 &= \frac{\partial}{\partial x} h_2(0, 0, 0, 0) = -\frac{1}{3} \\ a_4 &= \frac{\partial}{\partial x} h_4(0, 0, 0, 0) = 0 & a_5 &= h_6(0, 0, 0, 0) = 0. \end{aligned}$$

Furthermore, we can define the quantity:

$$A = -a_2 + 3a_3 - (2a_4 + 2a_5) = -1,$$

which is important in the following analysis, in particular for $A \neq 0$ (Krupa & Szmolyan 2001). Similar to the procedure in Section 4, sections of the dynamical system can be defined, in order to monitor the in- and outgoing trajectories. In this case we are interested in two sections of the neighbourhood U , defined as in Section 4, that monitor S^a and S^r close to the fold point. Let $\Delta_a = \{(x, \rho^2), x \in I_a\}$ and $\Delta_r = \{(x, \rho^2), x \in I_r\}$, where I_a, I_r are intervals on the real line and ρ is sufficiently small. Furthermore, define q_a to be the point on Δ_a that belongs to the attracting branch S^a , while q_r is equivalently defined as the point on Δ_r that corresponds to S^r . Finally, we are in the position to define the transition map $\pi : \Delta^a \rightarrow \Delta^r$, compare to Section 4. Following this, Krupa & Szmolyan (2001) discuss the existence of a critical value for λ (denoted λ_c), where the two branches S_r and S_a must connect in a smooth fashion. The transition map π has to map the point q_a to q_r , if the branches are connected, and the trajectory passing through the fold point is called the maximal canard, see Definition 5.2. The following theorem describes the technical details involved, and some of the results are derived by the following analysis.

Theorem 5.4 (Krupa & Szmolyan (2001))

Assume that system (3.1) satisfies the defining non-degeneracy conditions (Equations 24 and 25) of a canard

point. Assume that the solution $x_0(t)$ of the reduced problem connects S_a to S_r . Then there exists $\epsilon_0 > 0$ and a smooth function $\lambda_c(\sqrt{\epsilon})$ defined on $[0, \epsilon_0]$ such that for $\epsilon \in (0, \epsilon_0)$ the following assertions hold:

- $\pi(q_{a,\epsilon}) = q_{r,\epsilon}$ iff $\lambda = \lambda_c(\sqrt{\epsilon})$.

- The function λ_c has the expansion

$$\lambda_c(\sqrt{\epsilon}) = -\epsilon \left(\frac{a_1 + a_5}{2} + \frac{A}{8} \right) + O(\epsilon^{\frac{3}{2}}).$$

- The transition map π is defined only for λ in an interval around $\lambda_c(\sqrt{\epsilon})$ of width $O(\exp(-\frac{c}{\epsilon}))$ for some $c > 0$.

$$\frac{\partial}{\partial \lambda} (\pi(q_{a,\epsilon}) - q_{r,\epsilon})|_{\lambda=\lambda_c(\sqrt{\epsilon})} > 0$$

5.1 Canard Blow-up

Now similarly to Section 4, we consider a transformations of the coordinate system in order to analyse the dynamics in the neighbourhood of the non-hyperbolic equilibrium induced by the canard point. The transformations are taken from (Krupa & Szmolyan 2001) and are,

$$x = \bar{r}\bar{x}, \quad y = \bar{r}^2y, \quad \epsilon = \bar{r}^2\bar{\epsilon}, \quad \lambda = \bar{r}\bar{\lambda}. \quad (28)$$

Now that we have established these transformation, the charts K_1 and K_2 can be introduced, but it is not necessary to consider the third chart, K_3 . Since the attracting slow manifold connects to the repelling slow manifold, the flow will ‘bend back’ from K_2 into K_1 instead of leaving the neighbourhood U in the direction of the fast flow, which was described by K_3 in Section 4. This pheonomenon can be observed in Figure 10, where the trajectory stays close to S^r after passing the fold point.

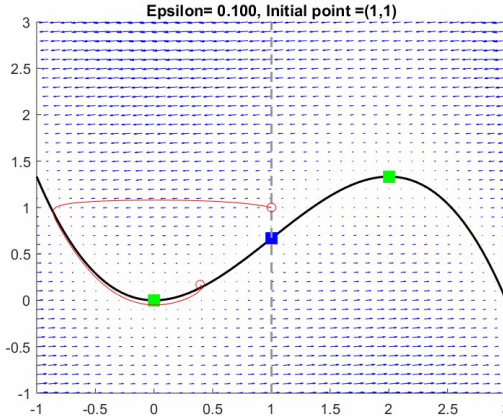


Figure 10: The Van der Pol system for the canard case.

Again, equivalently to the procedure in Section 4, we can define the coordinate transformation for the charts. Note, that in contrast to the generic Blow-Up in Section 4, the coordinate system is now in \mathbf{R}^4 , and not in \mathbf{R}^3 . In chart K_1 , $y_1 = 1$, while in K_2 , $\epsilon_1 = 1$ and then:

$$x = r_1 x_1, \quad y = r_1^2, \quad \epsilon = r_1^2 \epsilon_1, \quad \lambda = r_1 \lambda_1 \quad (29a)$$

$$x = r_2 x_2, \quad y = r_2^2 y_2, \quad \epsilon = r_2^2, \quad \lambda = r_2 \lambda_2. \quad (29b)$$

Furthermore, we can define the coordinate change between the two charts as follows:

Lemma 5.5

Let κ_{12} denote the change of coordinates from K_1 to K_2 . Then κ_{12} is given by

$$x_2 = x_1 \epsilon_1^{-1/2}, \quad y_2 = \epsilon_1^{-1}, \quad r_2 = r_1 \epsilon_1^{1/2}, \quad \lambda_2 = \epsilon_1^{-1/2} \lambda_1,$$

for $\epsilon_1 > 0$. Similarly $\kappa_{21} = \kappa_{12}^{-1}$ is given by

$$x_1 = x_2 y_2^{-1/2}, \quad r_1 = r_2 y_2^{1/2}, \quad \epsilon_1 = y_2^{-1}, \quad \lambda_1 = \lambda_2 y_2^{-1/2},$$

for $y_2 > 0$.

We are now in the position to begin with the analysis in the charts, and will first consider chart K_2 , since, as in Section 4, K_2 holds the most information.

5.1.1 Dynamics in K_2

We start by noting that we are considering our invariant plane at $r_2 = 0$ which will significantly simplify our system for K_2 . Further we should note that we are taking a transformation in time, $\frac{dr}{dt_2} = \frac{dt}{dt_2} \frac{dr}{dt} = \frac{1}{r_2} \frac{dr}{dt}$, as well as in our coordinates. Then if we substitute our time transformation and Equation 29b into our system of Equations 26 we find,

$$\begin{aligned} r_2^2 x'_2 - r_2 x_2 r'_2 &= -r_2^2 y_2 h_1 + r_2^2 x_2^2 h_2, \\ \implies x'_2 &= -y_2 + x_2^2 - r_2 G_2(x_2, y_2), \end{aligned} \quad (30a)$$

$$\begin{aligned} r_2^3 y'_2 - 3r_2^2 y_2 r'_2 &= r_2^2 (r_2 x_2 h_4 - r_2 \lambda_2 h_5), \\ \implies y'_2 &= x_2 - \lambda_2 + r_2 G_2(x_2, y_2), \end{aligned} \quad (30b)$$

where we note that $h_j = h_j(x, y, \epsilon, \lambda)$ for $j = 1, 2, 3, 4, 5$. Notice that we have included an additional term in Equation 30 - we define $G_2(x_2, y_2)$ in the following way, $G(x_2, y_2) = (G_1(x_2, y_2), G_2(x_2, y_2))^T = (-\frac{x_2^3}{3}, 0)^T$. The reason we also define this vector is to aide in the Melnikov computations which we will see later. Then combining this yields our complete system

$$x'_2 = -y_2 + x_2^2 - r_2 G_1(x_2, y_2) = -y_2 + x_2^2 - r_2 \left(-\frac{x_2^3}{3} \right), \quad (30a)$$

$$y'_2 = x_2 - \lambda_2 + r_2 G_2(x_2, y_2) = x_2 - \lambda_2, \quad (30b)$$

recalling that $r'_2 = \lambda'_2 = 0$. Moreover, Krupa & Szmolyan (2001) discusses that for this chart we have an interesting result. They note that at $r_2 = \lambda_2 = 0$ our system is integrable which allows us to define a constant of motion $H(x_2, y_2) = \frac{1}{2} \exp(-2y_2) (y_2 - x_2^2 + \frac{1}{2})$. For clarity we will first proceed with deriving this equation

of motion. Firstly, multiply each equations by, $e^{2y_2}e^{-2y_2} = 1$, and define sections of each equation as partial derivatives of H such that ,

$$x'_2 = e^{2y_2}e^{-2y_2}(-y_2 + x_2^2) = e^{2y_2} \frac{\partial H}{\partial y_2}(x_2, y_2) \quad (32)$$

$$y'_2 = -e^{2y_2}e^{-2y_2}(-x_2) = -e^{2y_2} \frac{\partial H}{\partial x_2}(x_2, y_2). \quad (33)$$

Then we integrate $\frac{\partial H}{\partial x_2}(x_2, y_2) = -e^{-2y_2}x_2$ to give,

$$H(x_2, y_2) = -\frac{1}{2}x^2e^{-2y_2} + C(y),$$

where $C(y)$ is the constant of integration, which depends on y . Then, by taking the derivative with respect to y and setting it equal to the expression $\frac{\partial H}{\partial y_2}(x_2, y_2) = e^{-2y_2}(-y_2 + x_2^2)$, we can find the value for $C(y)$ as follows:

$$\begin{aligned} \frac{\partial H}{\partial y_2}(x_2, y_2) &= x^2e^{-2y_2} + C'(y) \\ \Rightarrow C'(y) &= -y_2e^{-2y_2} \end{aligned}$$

Finally we integrate $C'(y)$ in order to find an explicit expression for H ,

$$C(y) = \int -y_2e^{-2y_2}dy = \frac{1}{2}y_2e^{-2y_2} + \frac{1}{2}e^{-2y_2} + const,$$

using integration by parts. Then, the final expression is:

$$\begin{aligned} H(x_2, y_2) &= -\frac{1}{2}x^2e^{-2y_2} + \frac{1}{2}y_2e^{-2y_2} + \frac{1}{2}e^{-2y_2} + c \\ &= \frac{1}{2}e^{-2y_2} \left(y_2 - x_2^2 + \frac{1}{2} \right) + c. \end{aligned}$$

Note that without loss of generality we can choose $c = 0$ because we are interested in the level curves of H and $H = h$. Now that we have shown how the constant of motion is constructed we will consider our reduced system, that we have an equilibrium at the origin, implying that $H(x_2, y_2) = h$. Considering the reduced system (Equation 30) we have from $H(x_2, y_2) = 0$ that,

$$x'_2 = \frac{1}{2} \implies x_2 = \frac{t_2}{2} + A, \quad (34a)$$

$$y'_2 = \frac{t_2}{2} \implies y_2 = \frac{t_2^2}{4} - \frac{1}{2}, \quad (34b)$$

where we have directly integrated Equation 34a with respect to our time (t_2). However, we note that we are able to choose $A = 0$, as we are considering an autonomous (time-invariant) system. Then for Equation 34b we are able to rearrange the constant of motion at zero to give, $y_2 = x_2^2 - \frac{1}{2}$. Clearly from this analysis we are then able to define our trajectories in terms of $\gamma_{c,2}$,

$$\gamma_{c,2}(t_2) = (x_{c,2}(t_2), y_{c,2}(t_2)) = \left(\frac{t_2}{2}, \frac{t_2^2}{4} - \frac{1}{2} \right). \quad (35)$$

Now that we have established that we must have a flow on our second chart, then there must also exist transition maps. Therefore this now enables us to consider the first chart in the following section.

5.1.2 Dynamics in K_1

For K_1 we follow a similar approach to the above. We will use the transformations,

$$x = r_1 x_1, \quad y = r_1^2, \quad \epsilon = r_1^2 \epsilon_1, \quad \lambda = r_1 \lambda_1, \quad (29a)$$

to find the relevant pathways of our flows. Now if we first consider the r_1 component,

$$2r_1^2 r'_1 = r_1^2 \epsilon (r_1 x_1 - r_1 \lambda_1), \quad (36)$$

where we define $F = F(x, y, \epsilon, \lambda) = x_1 - \lambda_1 + O(r_1(r_1 + \lambda_1))$. Next we consider $x = r_1 x_1$,

$$\begin{aligned} r_1 r'_1 x_1 + r_1^2 x'_1 &= -r_1^2 + r_1^2 x_1^2, \\ x'_1 &= -1 + x_1^2 - \frac{x_1 r'_1}{r_1}, \end{aligned}$$

where we can use Equation 36 to simplify this further,

$$x'_1 = -1 + x_1^2 - \frac{x_1}{r_1} \left(\frac{r_1 \epsilon_1 F}{2} \right). \quad (37)$$

We now consider $\epsilon = \epsilon_1 r_1^2$ and noting $\epsilon' = 0$. Then we have, $r_1^3 \epsilon' = -2r_1^2 \epsilon_1 r'_1$, where we can use Equation 36 to simplify to,

$$\epsilon' = -\epsilon_1^2 F. \quad (38)$$

Our last transformation is for our new coordinate $\lambda = r_1 \lambda$, noting that $\lambda' = 0$. Similarly to the above we find $r_1^2 \lambda'_1 + r_1 \lambda_1 r'_1 = 0$ then,

$$\lambda'_1 = -\frac{\lambda_1 \epsilon_1 F}{2}, \quad (39)$$

which is a trivial rearrangement as seen in Equation 38. Now if we combine the above we find that our transformed system is of the following form,

$$r'_1 = \frac{\epsilon}{2} (r_1 x_1 - r_1 \lambda_1), \quad (40a)$$

$$x'_1 = -1 + x_1^2 - \frac{x_1 \epsilon_1 F}{2}, \quad (40b)$$

$$\epsilon' = -\epsilon_1^2 F, \quad (40c)$$

$$\lambda'_1 = -\frac{\lambda_1 \epsilon_1 F}{2}. \quad (40d)$$

From this system we are now able to make some deductions. We first can observe that the hyperplanes are along the $r_1 = \epsilon_1 = \lambda_1 = 0$ with an invariant line at $l_1 = \{(x_1, 0, 0, 0) : x_1 \in \mathbb{R}\}$ (Krupa & Szmolyan 2001). As Krupa & Szmolyan (2001) discusses the equilibria present at the end of both of our branches - Figure 9 - which are found at $p_a = (-1, 0, 0, 0)$ and $p_r = (1, 0, 0, 0)$ (Krupa & Szmolyan 2001). Now we can go one step further, we can consider Equation 40 and find the eigenvalues of the system for the invariant planes. We find that,

$$J - \sigma I = \begin{bmatrix} 2x - \sigma & 0 & 0 & 0 \\ 0 & -\sigma & 0 & 0 \\ 0 & 0 & -\sigma & 0 \\ 0 & 0 & 0 & -\sigma \end{bmatrix}, \quad (41)$$

which clearly has three zero eigenvalues and one non-zero eigenvalue $\sigma = \pm 2$. Which further emphasises that our equilibrium point is non-hyperbolic. As a result we intuitively expect that something interesting occurs at this point. In the section following we will be considering what effect these mappings and eigenvalues will have on our system.

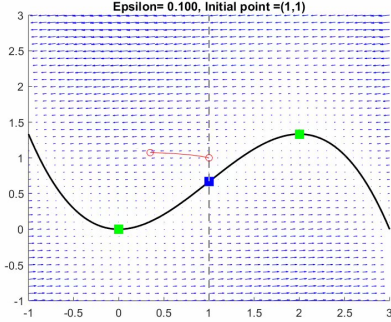
5.2 Effect of the Canard Point

Now that we have shown that there must exist a flow around our fold point we should now consider the global effect of the canard point. We can see by considering the system of Equations 40 that our equilibriums are at $(x, y) = (\lambda, \lambda^2[\frac{1-\lambda}{3}])$ and find the eigenvalues from the matrix,

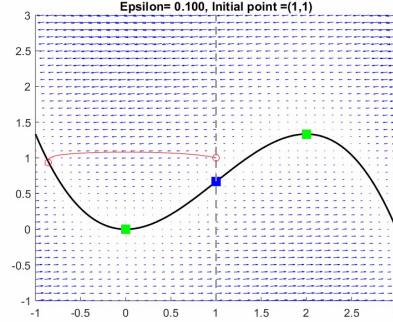
$$A - \sigma I = \begin{bmatrix} 2x - x^2 - \sigma & -1 & 0 & 0 \\ \epsilon & -\sigma & x - \lambda & -\epsilon \\ 0 & 0 & -\sigma & 0 \\ 0 & 0 & 0 & -\sigma \end{bmatrix} = \sigma^2(\sigma^2 + \sigma(x^2 - 2x) + \epsilon). \quad (42)$$

From this we are about to find the eigenvalues of the system, $\sigma = 0$ and $\sigma = \frac{2x-x^2 \pm \sqrt{(x^2-2x)^2-4\epsilon}}{2}$. Then we consider the values at our equilibrium, $x = \lambda$, to find that we have a Hopf Bifurcation when $4\epsilon > (x^2 - 2x)^2$ or when $\lambda = 2$ or 0 . This then leads to the following trajectories within the flow - Figure 11.

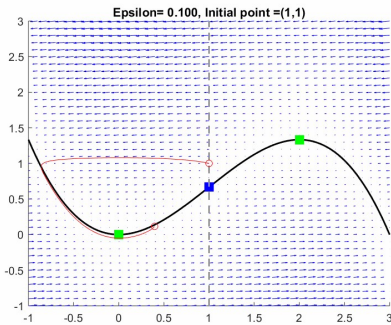
5. CANARD IN TWO DIMENSIONS



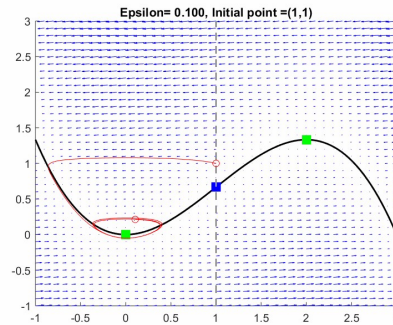
(a) The initial flow within the system.



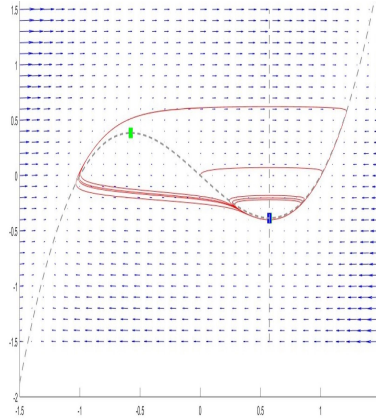
(b) The flow as it hits the slow manifold.



(c) The flow as it intersects with the fold point.



(d) The Hopf bifurcation due to the canard point.



(e) Growth of the Hopf bifurcation leading to the formation of a Canard explosion.

Figure 11: The trajectories associated with the canards case of the Van der Pol system.

From Figure 11 we can see the progression of our flow over the system. From Figure 11a we see that the flow starts at an initial condition of $(x, y) = (1, 1)$ and travels along the fast flow towards the attracting branch. Then from Figure 11b the flow has hit the attracting branch, where it then follows along the slow flow towards the

fold point at $(x, y) = (0, 0)$, which is described by Figure 11c. Then from Figures 11c and 11d we can observe the Hopf bifurcation. This is because we make note that the canard point is present at $-\lambda$, which in essence pushes the flow up the repelling branch (see Figure 9) until the flow is sufficiently far from the fold point where it will then repel towards the attracting branch, starting the growing oscillations - Figure 11d. When the Hopf bifurcation is large we would then expect to see a jump in our solution to an attracting branch - Figure 11e.

5.2.1 Separation of the Manifolds

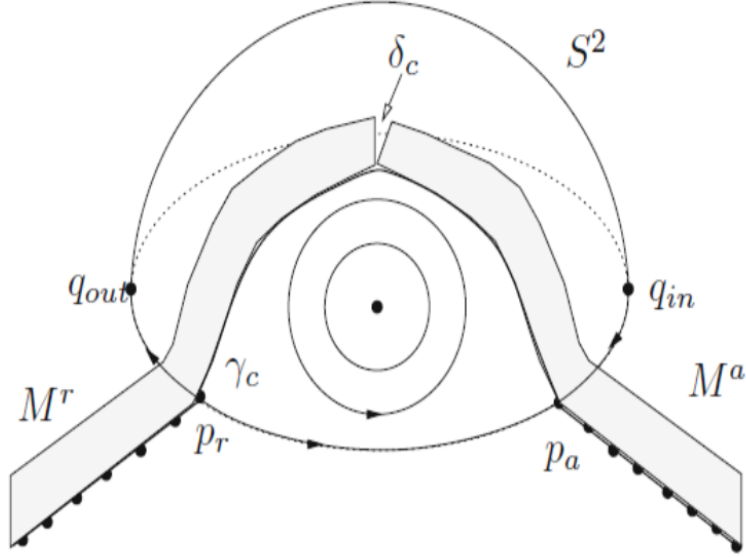


Figure 12: Separation of M_a and M_r (Kuehn 2015).

Continuing on from the singular Hopf bifurcation we might find that the canard point forces our branches to split. In other words we are looking for when the attracting and repelling branches are no longer connected, as shown in Figure 12. To do this we would use Melnikov Computations to show that our manifolds split - see *Extending Geometric Singular Perturbation Theory to Nonhyperbolic Points - Fold and Canard Points in Two Dimensions* (Krupa & Szmolyan 2001) for direct use. To discover whether we have a splitting between our branches we need to consider our y coordinates with respect to our second chart such that $y_{a,2}(0) - y_{r,2}(0)$ is a distance function which can be written as $D_c(r_2, \lambda_2) = H(0, y_{a,2}(0)) - H(0, y_{r,2}(0))$ as we note that $\frac{\partial}{\partial y_2} H(0, y_2) \neq 0$ (Krupa & Szmolyan 2001). From here we can use the following proposition,

Proposition 5.6 (Krupa & Szmolyan 2001)

For a small enough ρ and μ the distance function has the expansion

$$D_c(r_2, \lambda_2) = d_{r_2} r_2 + d_{\lambda_2} \lambda_2 + O(2),$$

where we have defined,

$$d_{r_2} = \int_{-\infty}^{\infty} \text{grad}H(\gamma_{c,2}(t)) \cdot G(\gamma_{c,2}(t)) dt, \quad (43a)$$

$$d_{\lambda_2} = \int_{-\infty}^{\infty} \text{grad}H(\gamma_{c,2}(t)) \cdot (0, -1)^T, \quad (43b)$$

and our matrix $G(\gamma_{c,2}(t))$ in Section 5.1.2 with $\gamma_{c,2}$ as our critical trajectory.

Then, following the proof provided by Krupa & Szmolyan (2001), we find that we will have a split occurring between our branches if the canard falls outside of our domain of order $O(e^{-\frac{c}{\epsilon}})$ such that $D_c(r_2, \lambda_2) \neq 0$. As a result of we see a flow similar to Figure 12 whereby we find that our flow could either jump off under the fast flow - see Figure 8 - or we might find that the flow could be trapped in the canard region and then be repelled back to the attracting manifold, as we see with our connected system - Figure 11.

Good to have a figure if possible

6 Canards in Three Dimensions

++++++change name of chapter++++++

Canards in two dimensional fast-slow systems are degenerate phenomena, while they generically occur in higher dimensional systems. This means that while in two dimensional systems canards only occur in $O(\epsilon)$ is parameter space, they occur for $O(1)$ in parameter space in a three dimensional system and are therefore more robust. In the following two sections we consider three dimensional fast slow systems with one fast and two slow variables,

$$\begin{cases} \epsilon \dot{x} = f(x, y, z, y, \epsilon), \\ \dot{y} = g_1(x, y, z, y, \epsilon), \\ \dot{z} = g_2(x, y, z, y, \epsilon), \end{cases} \quad (44)$$

which can be seen as an application of the original form of the fast-slow system (2), with $n = 1, m = 2$ (Desroches et al. 2012). The analysis is of a similar structure as for the two dimensional case.

We can identify the points that will cause complication for the analysis of the system by considering the nondegeneracy conditions as in the two dimensional case. Here, the slightly extended version is

$$\begin{aligned} f(p_*, \lambda, 0) &= 0, \\ \frac{\partial}{\partial x} f(p_*, \lambda, 0) &= 0, \\ \frac{\partial^2}{\partial x^2} f(p_*, \lambda, 0) &\neq 0, \\ D_{(y,z)} f(p_*, \lambda, 0) &\text{ has full rank one,} \end{aligned} \quad (45)$$

where $p_* = (x_*, y_*, z_*) \in F$ denotes ther fold points and $D_{(y,z)} = (\frac{\partial f}{\partial y}, \frac{\partial f}{\partial z})$ (Desroches et al. 2012). This gives rise to a fold line, on which all of the p^* lie. This consequence is immediately obvious by considering Figure 16, and taking the two dimensional Van der Pol system as a crosssection of the two dimensional plane. Then the two fold points in the two dimensional case extend to two fold lines in the three dimensional case.

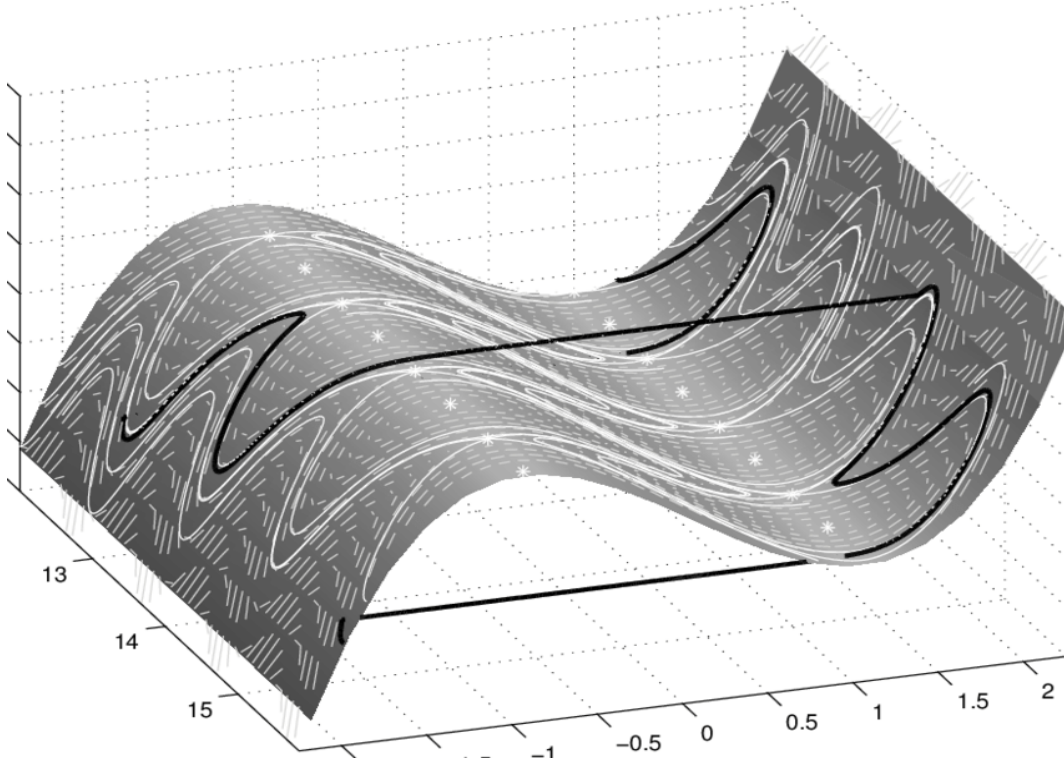


Figure 13: Three dimensional Van der Pol ([Festschrift et al. 2001](#)).

In order to find the points that are classified as folded singularities, denoted by * in Figure 16, which give rise to canard solutions, further analysis has to be carried out. The criterion we need is the fact that a folded singularity coincides with an equilibrium of the desingularised reduced problem. Therefore, we focus on the reduced system, which is as in the two dimensional case the slow system (58), in the singular limit $\epsilon \rightarrow 0$:

$$\begin{cases} 0 &= f(x, y, z, y, \epsilon), \\ \dot{y} &= g_1(x, y, z, y, \epsilon), \\ \dot{z} &= g_2(x, y, z, y, \epsilon), \end{cases} \quad (46)$$

Now, taking the total derivative of f results in

$$0 = \frac{\partial f}{\partial t} = \dot{y} \frac{\partial f}{\partial y} + \dot{z} \frac{\partial f}{\partial z} + \dot{x} \frac{\partial f}{\partial x}.$$

Then, rearranging for the term including \dot{x} and noting that $y' = g_1$ and $z' = g_2$ results in

$$-\dot{x} \frac{\partial f}{\partial x} = g_1 \frac{\partial f}{\partial y} + g_2 \frac{\partial f}{\partial z}.$$

This is almost of the desired form, however, we cannot divide by $-\frac{\partial f}{\partial x}$ to get an expression for \dot{x} , since $\frac{\partial f}{\partial x}(p^*) = 0$, from the nondegeneracy condition. Therefore, as in the two dimensional case, we apply a rescaling of time in terms of $-\frac{\partial f}{\partial x}$, such that:

$$\begin{cases} \dot{x} &= g_1 \frac{\partial f}{\partial y} + g_2 \frac{\partial f}{\partial z}, \\ \dot{y} &= -g_1 \frac{\partial f}{\partial x}, \\ \dot{z} &= -g_2 \frac{\partial f}{\partial x}. \end{cases} \quad (47)$$

This is the desingularised reduced system, and its equilibrium satisfies

$$l(p^*) = g_1(p_*, \lambda, 0) \frac{\partial}{\partial y} f(p_*, \lambda, 0) + g_2(p_*, \lambda, 0) \frac{\partial}{\partial z} f(p_*, \lambda, 0) = 0.$$

This is where the so called normal switching condition $l(p^*) \neq 0$ fails ((?)).

The next step is to consider the nature of the folded singularity. This has not been as relevant in the two dimensional system, however, in the three dimensional case, the type of equilibrium the reduced system possesses determines the type and number of canards that can be observed in the full system. Therefore, we consider the three dimensional Jacobian,

$$J = \begin{bmatrix} \frac{\partial \dot{x}}{\partial x} & \frac{\partial \dot{x}}{\partial y} & \frac{\partial \dot{x}}{\partial z} \\ \frac{\partial \dot{y}}{\partial x} & \frac{\partial \dot{y}}{\partial y} & \frac{\partial \dot{y}}{\partial z} \\ \frac{\partial \dot{z}}{\partial x} & \frac{\partial \dot{z}}{\partial y} & \frac{\partial \dot{z}}{\partial z} \end{bmatrix}, \quad (48)$$

The resulting three eigenvalues, σ_i for $i = 1, 2, 3$ ([Desroches et al. 2012](#)) determine the stability of the folded singularity. Without loss of generality we can choose $\sigma_3 = 0$ because at least one of the eigenvalues must be zero to account for the folded singularity. The other two eigenvalues can be defined as the weak and strong eigenvalues, corresponding to the weak and strong canards, introduced below. The classification of the eigenvalues is done as follows: $|\sigma_1| > |\sigma_2| \iff |\sigma_s| > |\sigma_w|$, i.e. the greater eigenvalue, in modulus, is defined as the strong eigenvalue and vice versa. We can define the eigenvalue ratio $\mu := \frac{\sigma_w}{\sigma_s}$, which will be an important We can infer from standard stability theory that the folded singularity can have three types of stability, classified as follows:

$$\begin{cases} Saddle \ \sigma_1 \sigma_2 < 0 : \sigma_i \in \Re, \\ Node \ \sigma_1 \sigma_2 > 0 : \sigma_i \in \Re, \\ Focus \ \sigma_1 \sigma_2 > 0 : \Im(\sigma_i) \neq 0, \end{cases} \quad (49)$$

([Desroches et al. 2012](#)).

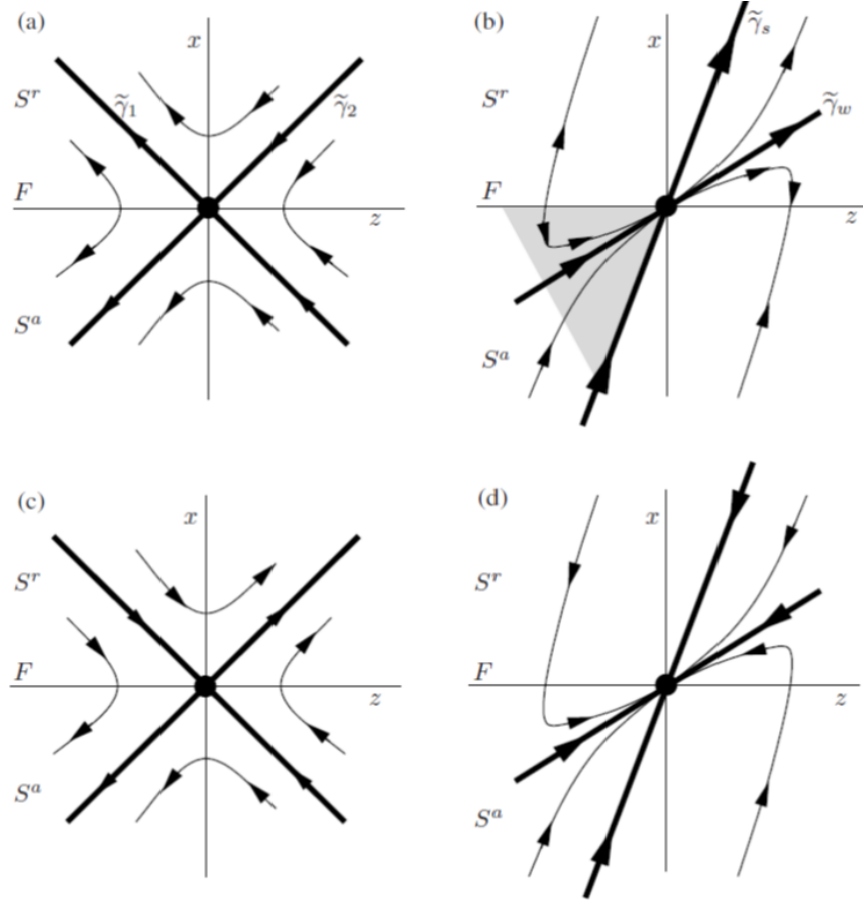


Figure 14: Phase portraits of our three dimensional system where a) is a folded saddle, b) folded node, c) and d) are desingularised flows ([Desroches et al. 2012](#)).

Two of the three types of equilibria are illustrated in Figure 17, where the effect of the desingularisation is displayed as well. The scaling by $-\frac{\partial f}{\partial x}$ causes a reversal of the arrows in the repelling sheet S^r , which allows the two trajectories passing through the folded singularity to connect the attracting and repelling sheet which is not possible before desingularisation. These connecting trajectories are called singular canards.

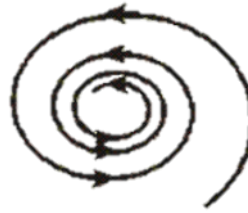


Figure 15: The branches of a spiral ([International Technological University n.d.](#)).

It should be noted that a singular canard is only present if the node or saddle connects the attracting and repelling sheets S^r and S^a . However, for the focus equilibrium we are unable to construct branches which connect, since the trajectories are spiralling towards or away from the equilibrium, consider Figure 18. Then, desingularising the flow, which causes the reversal of the flow on the repelling sheet will only have the effect that the spiralling trajectories cannot cross the fold. Therefore, there are no singular canards present in the case of a folded focus.

The following theorem summarises the findings for the different types of equilibria and the presence of canards in three dimensions:

Theorem 6.1 (Canards in \mathbf{R}^3 ([Desroches et al. 2012](#)))

For slow-fast systems (Equation 58) with $\epsilon > 0$ sufficiently small the following holds:

1. There are no maximal canards generated by a folded focus. For a folded saddle the two singular canards $\gamma_{1,2}$ perturb to maximal canards $\gamma_{1,2}$.
2. For a folded node let $\mu = \frac{\sigma_w}{\sigma_s} < 1$. the singular canard $\bar{\gamma}_s$ (“the strong canard”) always perturbs to a maximal canard γ_s . If $\mu^{-1} \notin \mathbb{N}$, then the singular canard $\bar{\gamma}_w$ (“weak canard”) also perturbs to a maximal canard. We call γ_s and γ_w primary canards.
3. For a folded node suppose $k > 0$ is an integer such that $2k+1 < \mu^{-1} < 2k+3$ and $\mu^{-1} \neq 2(k+1)$. Then, in addition to $\gamma_{s,w}$ there are k other maximal canards, which we call secondary canard.
4. The primary weak canard of a node undergoes a transcritical bifurcation for odd $\mu^{-1} \in \mathbb{N}$ and a pitchfork bifurcation for even $\mu^{-1} \in \mathbb{N}$

This theorem summarises the findings for different types of folded singularities. It establishes the persistence of the singular canards as maximal canards of the full system $\epsilon > 0$ for the different types of singularities. Furthermore, it provides a tool for calculating the number of secondary canards present in the full system, additional to the primary canards γ_s and γ_w . For $\mu^{-1} \in \mathbb{N}$ bifurcations occur and the number of secondary canards present varies according to the type of bifurcation. These mechanisms are best understood in the case of a folded node, which is studied in the following section.

6.1 The Folded Node

In this section the occurrence of canards and small amplitude oscillations due to a folded node of the reduced system is discussed. For a full presentation of canards in three dimensions for a folded node, see ([Wechselberger 2005](#)). The folded node singularity is an equilibrium of the reduced system. Note that it is only defined on S , the critical manifold and therefore only for the slow flow. There is no global equilibrium for the normal form introduced below, which will become apparent in this section. The normal form considered for analysing the folded node singularity is

$$\begin{aligned}\epsilon \dot{x} &= y - x^2 \\ \dot{y} &= -z - (\mu + 1)x \\ \dot{z} &= \frac{1}{2}\mu\end{aligned}\tag{50}$$

where μ is the eigenvalue ratio from before.

Note here that the reason that no global equilibrium exists is because system (64) can only have an equilibrium if $z = 0$. This would imply that $\mu = 0$. However, as the classification of folded singularities has shown, since

$\sigma_1\sigma_2 > 0$, $\mu \neq 0$ for the folded node. It is now of interest to verify the location of the folded singularity at the origin, and therefore derive the reduced system as well as the eigenvalues for the reduced problem. This is a simple application of the theory introduced earlier in this section. Consider equation (64) and define $\dot{x} := f$ as before. When $\epsilon \rightarrow 0$ in system (64), it follows that $f = y - x^2 = 0$, and therefore the critical manifold is defined as $S := \{(x, y, z) : y = x^2\}$, which is a folded two dimensional plane. Now that f is defined explicitly, we can check the nondegeneracy conditions for a folded singularity, as presented in (59) and get the following results:

$$\begin{aligned} f(x, y, z, \mu, \epsilon) &= 0 \\ \Rightarrow y &= x^2 \end{aligned}$$

$$\begin{aligned} \frac{\partial f}{\partial x}(x, y, z, \mu, \epsilon) &= 2x = 0 \\ \Rightarrow x &= 0 \Rightarrow y = 0 \\ \frac{\partial^2 f}{\partial x^2}(x, y, z, \mu, \epsilon) &= 2 \neq 0 \\ D_{(y,z)}f &= (1, 0) \text{ full rank one.} \end{aligned}$$

This shows that there exists a fold line $L := (0, 0, z)$ on the slow manifold S . In order to determine at which value of z the folded node singularity is located, we have to consider the reduced system of (64). The aim is to find an equilibrium of the reduced problem, since we know from the theory discussed that the folded singularity is an equilibrium of the slow flow. The reduced problem is:

$$0 = y - x^2 := f \quad (51)$$

$$\dot{y} = -z - (\mu + 1)x \quad (52)$$

$$\dot{z} = \frac{1}{2}\mu \quad (53)$$

We are interested in the global dynamics of the slow system and therefore want to derive an expression for \dot{x} . In order to do so, as described earlier in this section, we take the total derivative of f and rearrange to get the following expression:

$$\dot{y} = 2x\dot{x}. \quad (54)$$

This can be rearranged to give an expression for the dynamics in x on the slow manifold:

$$\dot{x} = \frac{\dot{y}}{2x},$$

which is singular for $x = 0$, which coincides with the fold line. This can be desingularised by rescaling time in the whole reduced system by a factor of $2x$. This results in

$$\begin{aligned} \dot{x} &= -(\mu + 1)x - z \\ \dot{y} &= -2x(\mu + 1) - 2xz \\ \dot{z} &= x\mu, \end{aligned} \quad (55)$$

however, it can be noted that the equation for y can be omitted, since the change in y is directly related to the change in x by a factor of $2x$ as stated in equation (68). Therefore, the reduced dynamics can be sufficiently

described by

$$\begin{aligned}\dot{x} &= -(\mu + 1)x - z \\ \dot{z} &= x\mu.\end{aligned}\tag{56}$$

Now, following the theory for folded singularities, the folded node has to satisfy the condition $l(0, 0, z) = 0$

$$\begin{aligned}l(0, 0, z) &= -(\mu + 1)x - z = 0|_{(0, 0, z)} \\ \Rightarrow z &= 0,\end{aligned}$$

which leads to the conclusion that the folded singularity, defined on the slow manifold for $\epsilon \rightarrow 0$ and located on the fold line $L = (0, 0, z)$, is given by $(0, 0, 0)$, as expected. Note that in this case only one equilibrium of the reduced system exists, which is not generally the global case. The next step of the analysis is to verify that the folded singularity at the origin is indeed a folded node. As discussed in the beginning of Section 6, the classification of the singularities is determined by the eigenvalues of the reduced system. Therefore, the next step is calculating these eigenvalues. The Jacobian of the reduced system (70) is

$$J = \begin{bmatrix} -(\mu + 1) & -1 \\ \mu & 0 \end{bmatrix},\tag{57}$$

and therefore the characteristic equation yields

$$\begin{aligned}\sigma^2 + (\mu + 1)\sigma + \mu &= 0 \\ \Rightarrow \sigma_1 &= -1 \quad \text{and} \quad \sigma_2 = -\mu.\end{aligned}$$

Since μ is the eigenvalue ratio and satisfies $0 < \mu < 1$, we can conclude that

$$\sigma_1\sigma_2 = (-1)(-\mu) = \mu > 0,$$

and therefore, by the conditions presented earlier in this Section, this shows that the folded singularity is in fact a folded node. Note that if we had tried to find the eigenvalues for the full three dimensional reduced system (69) instead, an additional eigenvalue $\sigma_3 = 0$ would have occurred. This is the eigenvalue that corresponds to the loss of hyperbolicity at the folded node, which is expected for singular points.

In order to analyse the folded node, the system (??) is transformed using the blow up transformation $u = \epsilon^{1/2}\bar{x}$, $v = \epsilon\bar{y}$, $w = \epsilon^{1/2}\bar{z}$ and $\tau_1 = \epsilon^{1/2}\bar{t}$. Then, in a neighbourhood U of the folded node the system is represented by

$$\begin{aligned}\dot{x} &= \bar{y} - \bar{x}^2 \\ \dot{y} &= \bar{z} - \bar{x} \\ \dot{z} &= -\nu.\end{aligned}$$

In the following analysis, the bars will be omitted for readability. One important realisation is that the phase portraits for the rescaled system is topologically equivalent to the original normal form. Therefore, the mapping of solutions found in the blown up system to the original system is straightforward. ++++check if true++++ All the information needed to describe the dynamics near the fold point is now derived and therefore the next step in the analysis is the description of the SAOs. The SAOs in the folded node case are standard trajectories that follow a certain pattern. These patterns are, as discussed in Theorem 7.1, found by considering the eigenvalue

ratio μ . In the case of the folded node, μ satisfies $2k+1 < \mu^{-1} < 2k+3$. Solving for $k \in \mathbf{N}$, then k is the number of secondary canards ξ_i , where $i \in 1, \dots, k$, in the system as stated in Theorem 7.1. Furthermore, k corresponds to the number of twists the primary canard γ_s is performing around γ_w . A twist corresponds to a 180° rotation, see ?. It is important to note that $\mu^{-1} \notin \mathbf{N}$ in order to conclude the number of secondary canards. If $\mu^{-1} \in \mathbf{N}$, bifurcations occur and the number of secondary canards changes. For a full analysis of this phenomenon refer to (Wechselberger 2005).

These canards are trajectories that are entering the so called funnel region of the fold and contracted along the direction of S^a . This funnel region lies between the fold line L and the strong singular canard. It is represented by the grey region in Figure 17. For decreasing values of ϵ , the funnel becomes narrower and for $\epsilon \rightarrow 0$, all other canards converge to the strong singular canard. The number of SAOs an incoming trajectory undergoes depends on where the trajectory enters the fold region in the z plane. Different intervals I_i , $i \in 1, \dots, k$, of z can be defined according to how many SAOs will be observed in the interval. The interval in which the primary strong canard lies is significantly larger than the other intervals, so the secondary canards close to it will have a higher amplitude while the number of SAOs is smaller. As the number of SAOs increases, the amplitude of oscillations get smaller and are not readily visible. The result about the width of the intervals is summed up in the following theorem.

Theorem 6.2 (Width of Rotational Sectors)

[Desroches et al. 2012] Consider system (61) and assume it has a folded-node singularity. At an $O(1)$ distance from the fold curve, all secondary canards are in an $O(\epsilon^{(1-\mu)/2})$ neighbourhood of the primary strong canard. Hence, the width of the rotational sectors I_i , $1 \leq i \leq k$, is $O(\epsilon^{(1-\mu)/2})$ and the width of sector I_{k+1} is $O(1)$.

Insert the pictures for this section...

An illustrative example is provided in (Desroches et al. 2012), where $\mu \approx 0.0557$ and therefore $k = 8$. Therefore, besides the strong and weak primary canards γ_s and γ_w , there exist eight secondary canards ξ_i , where $i \in 1, \dots, 8$. Figure....+++ shows a small region of the phase space, which captures the intersection of the repelling and attracting sheet of the slow manifold. Furthermore, the region is bounded by two cross-sections Σ^a and Σ^{-a} . Another cross-section can be defined Σ^{fn} can be defined, and the flow in two dimensions is displayed in Figure....+++ In the Figure, the primary strong canard is illustrated in black, and the three strongest secondary canards are displayed as ξ_1 in orange, ξ_2 in magenta and ξ_3 in cyan. It is apparent that the primary strong canard makes twists around the center, where the weak canard is located. The secondary canards ξ_i , $i \in 4, \dots, 8$ as well as γ_w are present in the Figure as well. However, they are not visible, since they are increasingly close to each other in the middle.

The number of SAOs a trajectory undergoes is dependent on where it enters the funnel region in terms of the space variable z . The intervals that can be defined are I_0 up to I_9 , where I_0 is bounded by γ_s and much larger than the other intervals. The intervals I_1 up to i_8 is bounded by the corresponding number of secondary canards, and entering the fold region through the i th interval corresponds to i oscillations a trajectory undergoes. This is illustrated in Figure ++++

7 MMO

Canards in two dimensional fast-slow systems are degenerate phenomena, while they generically occur in higher dimensional systems. This means that while in two dimensional systems canards only occur in $O(\epsilon)$ is parameter space, they occur for $O(1)$ in parameter space in a three dimensional system and are therefore more robust. In

the following two sections we consider three dimensional fast slow systems with one fast and two slow variables,

$$\begin{cases} \epsilon \dot{x} = f(x, y, z, y, \epsilon), \\ \dot{y} = g_1(x, y, z, y, \epsilon), \\ \dot{z} = g_2(x, y, z, y, \epsilon), \end{cases} \quad (58)$$

which can be seen as an application of the original form of the fast-slow system (2), with $n = 1, m = 2$ ([Desroches et al. 2012](#)). The analysis is of a similar structure as for the two dimensional case.

We can identify the points that will cause complication for the analysis of the system by considering the nondegeneracy conditions as in the two dimensional case. Here, the slightly extended version is

$$\begin{aligned} f(p_*, \lambda, 0) &= 0, \\ \frac{\partial}{\partial x} f(p_*, \lambda, 0) &= 0, \\ \frac{\partial^2}{\partial x^2} f(p_*, \lambda, 0) &\neq 0, \\ D_{(y,z)} f(p_*, \lambda, 0) &\text{ has full rank one,} \end{aligned} \quad (59)$$

where $p_* = (x_*, y_*, z_*) \in F$ denotes the fold points and $D_{(y,z)} = (\frac{\partial f}{\partial y}, \frac{\partial f}{\partial z})$ ([Desroches et al. 2012](#)). This gives rise to a fold line, on which all of the p^* lie. This consequence is immediately obvious by considering Figure 16, and taking the two dimensional Van der Pol system as a crosssection of the two dimensional plane. Then the two fold points in the two dimensional case extend to two fold lines in the three dimensional case.

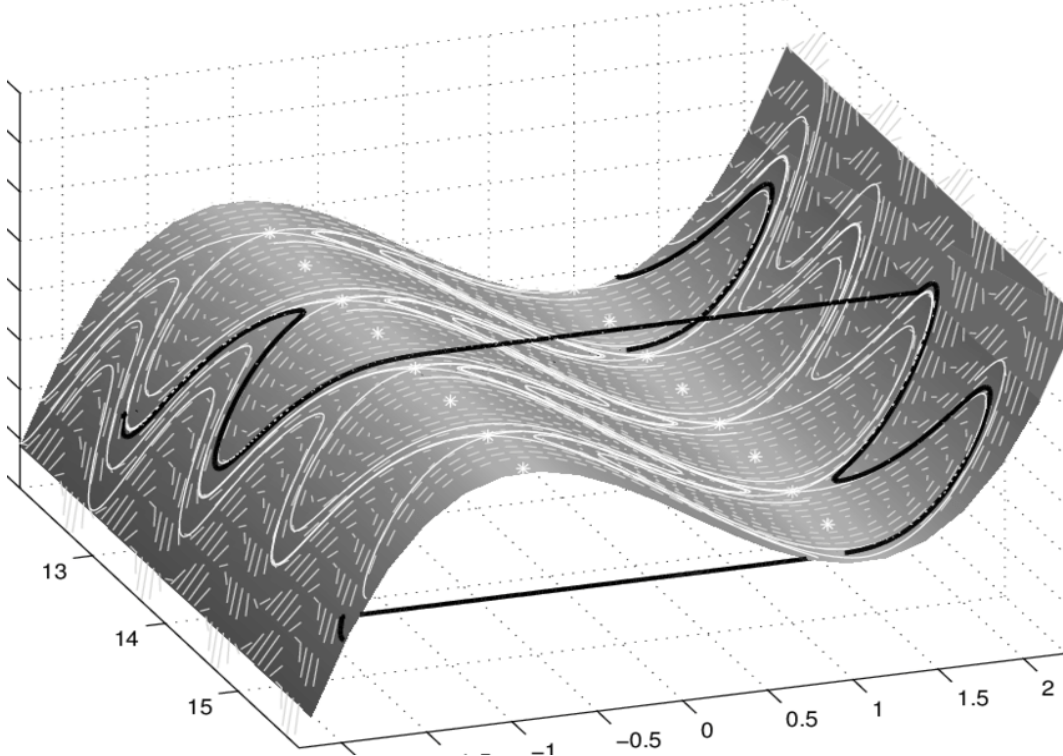


Figure 16: Three dimensional Van der Pol ([Festschrift et al. 2001](#)).

In order to find the points that are classified as folded singularities, denoted by * in Figure 16, which give rise to canard solutions, further analysis has to be carried out. The criterion we need is the fact that a folded singularity coincides with an equilibrium of the desingularised reduced problem. Therefore, we focus on the reduced system, which is as in the two dimensional case the slow system (58), in the singular limit $\epsilon \rightarrow 0$:

$$\begin{cases} 0 &= f(x, y, z, y, \epsilon), \\ \dot{y} &= g_1(x, y, z, y, \epsilon), \\ \dot{z} &= g_2(x, y, z, y, \epsilon), \end{cases} \quad (60)$$

Now, taking the total derivative of f results in

$$0 = \frac{\partial f}{\partial t} = \dot{y} \frac{\partial f}{\partial y} + \dot{z} \frac{\partial f}{\partial z} + \dot{x} \frac{\partial f}{\partial x}.$$

Then, rearranging for the term including \dot{x} and noting that $y' = g_1$ and $z' = g_2$ results in

$$-\dot{x} \frac{\partial f}{\partial x} = g_1 \frac{\partial f}{\partial y} + g_2 \frac{\partial f}{\partial z}.$$

This is almost of the desired form, however, we cannot divide by $-\frac{\partial f}{\partial x}$ to get an expression for \dot{x} , since $\frac{\partial f}{\partial x}(p^*) = 0$, from the nondegeneracy condition. Therefore, as in the two dimensional case, we apply a rescaling of time in terms of $-\frac{\partial f}{\partial x}$, such that:

$$\begin{cases} \dot{x} &= g_1 \frac{\partial f}{\partial y} + g_2 \frac{\partial f}{\partial z}, \\ \dot{y} &= -g_1 \frac{\partial f}{\partial x}, \\ \dot{z} &= -g_2 \frac{\partial f}{\partial x}. \end{cases} \quad (61)$$

This is the desingularised reduced system, and its equilibrium satisfies

$$l(p^*) = g_1(p^*, \lambda, 0) \frac{\partial}{\partial y} f(p^*, \lambda, 0) + g_2(p^*, \lambda, 0) \frac{\partial}{\partial z} f(p^*, \lambda, 0) = 0.$$

This is where the so called normal switching condition $l(p^*) \neq 0$ fails ((?)).

The next step is to consider the nature of the folded singularity. This has not been as relevant in the two dimensional system, however, in the three dimensional case, the type of equilibrium the reduced system possesses determines the type and number of canards that can be observed in the full system. Therefore, we consider the three dimensional Jacobian,

$$J = \begin{bmatrix} \frac{\partial \dot{x}}{\partial x} & \frac{\partial \dot{x}}{\partial y} & \frac{\partial \dot{x}}{\partial z} \\ \frac{\partial \dot{y}}{\partial x} & \frac{\partial \dot{y}}{\partial y} & \frac{\partial \dot{y}}{\partial z} \\ \frac{\partial \dot{z}}{\partial x} & \frac{\partial \dot{z}}{\partial y} & \frac{\partial \dot{z}}{\partial z} \end{bmatrix}, \quad (62)$$

The resulting three eigenvalues, σ_i for $i = 1, 2, 3$ ([Desroches et al. 2012](#)) determine the stability of the folded singularity. Without loss of generality we can choose $\sigma_3 = 0$ because at least one of the eigenvalues must be zero to account for the folded singularity. The other two eigenvalues can be defined as the weak and strong eigenvalues, corresponding to the weak and strong canards, introduced below. The classification of the eigenvalues is done as follows: $|\sigma_1| > |\sigma_2| \iff |\sigma_s| > |\sigma_w|$, i.e. the greater eigenvalue, in modulus, is defined as the strong eigenvalue and vice versa. We can define the eigenvalue ratio $\mu := \frac{\sigma_w}{\sigma_s}$, which will be an important We can infer from standard stability theory that the folded singularity can have three types of stability, classified as follows:

$$\begin{cases} \text{Saddle } \sigma_1 \sigma_2 < 0 : \sigma_i \in \Re, \\ \text{Node } \sigma_1 \sigma_2 > 0 : \sigma_i \in \Re, \\ \text{Focus } \sigma_1 \sigma_2 > 0 : \Im(\sigma_i) \neq 0, \end{cases} \quad (63)$$

([Desroches et al. 2012](#)).

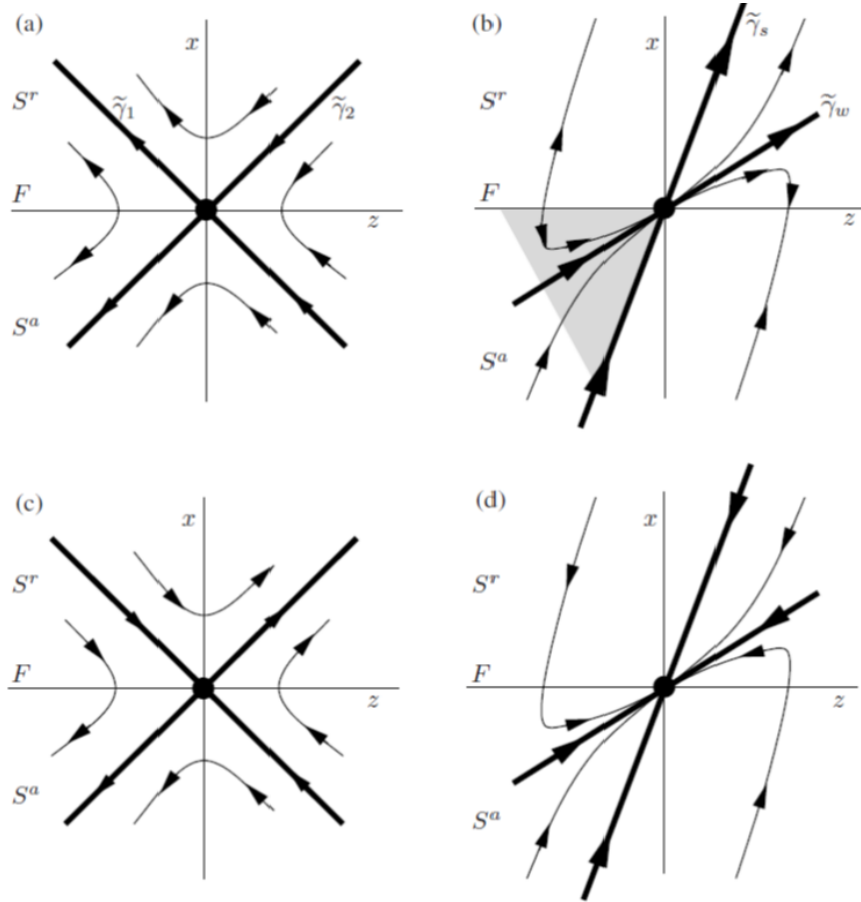


Figure 17: Phase portraits of our three dimensional system where a) is a folded saddle, b) folded node, c) and d) are desingularised flows ([Desroches et al. 2012](#)).

Two of the three types of equilibria are illustrated in Figure 17, where the effect of the desingularisation is displayed as well. The scaling by $-\frac{\partial f}{\partial x}$ causes a reversal of the arrows in the repelling sheet S^r , which allows the two trajectories passing through the folded singularity to connect the attracting and repelling sheet which is not possible before desingularisation. These connecting trajectories are called singular canards.

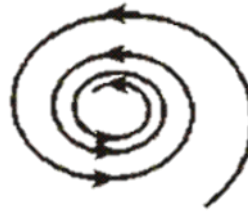


Figure 18: The branches of a spiral ([International Technological University n.d.](#)).

It should be noted that a singular canard is only present if the node or saddle connects the attracting and repelling sheets S^r and S^a . However, for the focus equilibrium we are unable to construct branches which connect, since the trajectories are spiralling towards or away from the equilibrium, consider Figure 18. Then, desingularising the flow, which causes the reversal of the flow on the repelling sheet will only have the effect that the spiralling trajectories cannot cross the fold. Therefore, there are no singular canards present in the case of a folded focus.

The following theorem summarises the findings for the different types of equilibria and the presence of canards in three dimensions:

Theorem 7.1 (Canards in \mathbf{R}^3 ([Desroches et al. 2012](#)))

For slow-fast systems (Equation 58) with $\epsilon > 0$ sufficiently small the following holds:

1. There are no maximal canards generated by a folded focus. For a folded saddle the two singular canards $\gamma_{1,2}$ perturb to maximal canards $\gamma_{1,2}$.
2. For a folded node let $\mu = \frac{\sigma_w}{\sigma_s} < 1$. the singular canard $\bar{\gamma}_s$ (“the strong canard”) always perturbs to a maximal canard γ_s . If $\mu^{-1} \notin \mathbb{N}$, then the singular canard $\bar{\gamma}_w$ (“weak canard”) also perturbs to a maximal canard. We call γ_s and γ_w primary canards.
3. For a folded node suppose $k > 0$ is an integer such that $2k+1 < \mu^{-1} < 2k+3$ and $\mu^{-1} \neq 2(k+1)$. Then, in addition to $\gamma_{s,w}$ there are k other maximal canards, which we call secondary canard.
4. The primary weak canard of a node undergoes a transcritical bifurcation for odd $\mu^{-1} \in \mathbb{N}$ and a pitchfork bifurcation for even $\mu^{-1} \in \mathbb{N}$

This theorem summarises the findings for different types of folded singularities. It establishes the persistence of the singular canards as maximal canards of the full system $\epsilon > 0$ for the different types of singularities. Furthermore, it provides a tool for calculating the number of secondary canards present in the full system, additional to the primary canards γ_s and γ_w . For $\mu^{-1} \in \mathbb{N}$ bifurcations occur and the number of secondary canards present varies according to the type of bifurcation. These mechanisms are best understood in the case of a folded node, which is studied in the following section.

7.1 The Folded Node

In this section the occurrence of canards and small amplitude oscillations due to a folded node of the reduced system is discussed. For a full presentation of canards in three dimensions for a folded node, see ([Wechselberger 2005](#)). The folded node singularity is an equilibrium of the reduced system. Note that it is only defined on S , the critical manifold and therefore only for the slow flow. There is no global equilibrium for the normal form introduced below, which will become apparent in this section. The normal form considered for analysing the folded node singularity is

$$\begin{aligned}\epsilon \dot{x} &= y - x^2 \\ \dot{y} &= -z - (\mu + 1)x \\ \dot{z} &= \frac{1}{2}\mu\end{aligned}\tag{64}$$

where μ is the eigenvalue ratio from before.

Note here that the reason that no global equilibrium exists is because system (64) can only have an equilibrium if $z = 0$. This would imply that $\mu = 0$. However, as the classification of folded singularities has shown, since

$\sigma_1\sigma_2 > 0$, $\mu \neq 0$ for the folded node. It is now of interest to verify the location of the folded singularity at the origin, and therefore derive the reduced system as well as the eigenvalues for the reduced problem. This is a simple application of the theory introduced earlier in this section. Consider equation (64) and define $\dot{x} := f$ as before. When $\epsilon \rightarrow 0$ in system (64), it follows that $f = y - x^2 = 0$, and therefore the critical manifold is defined as $S := \{(x, y, z) : y = x^2\}$, which is a folded two dimensional plane. Now that f is defined explicitly, we can check the nondegeneracy conditions for a folded singularity, as presented in (59) and get the following results:

$$\begin{aligned} f(x, y, z, \mu, \epsilon) &= 0 \\ \Rightarrow y &= x^2 \end{aligned}$$

$$\begin{aligned} \frac{\partial f}{\partial x}(x, y, z, \mu, \epsilon) &= 2x = 0 \\ \Rightarrow x &= 0 \Rightarrow y = 0 \\ \frac{\partial^2 f}{\partial x^2}(x, y, z, \mu, \epsilon) &= 2 \neq 0 \\ D_{(y,z)}f &= (1, 0) \text{ full rank one.} \end{aligned}$$

This shows that there exists a fold line $L := (0, 0, z)$ on the slow manifold S . In order to determine at which value of z the folded node singularity is located, we have to consider the reduced system of (64). The aim is to find an equilibrium of the reduced problem, since we know from the theory discussed that the folded singularity is an equilibrium of the slow flow. The reduced problem is:

$$0 = y - x^2 := f \quad (65)$$

$$\dot{y} = -z - (\mu + 1)x \quad (66)$$

$$\dot{z} = \frac{1}{2}\mu \quad (67)$$

We are interested in the global dynamics of the slow system and therefore want to derive an expression for \dot{x} . In order to do so, as described earlier in this section, we take the total derivative of f and rearrange to get the following expression:

$$\dot{y} = 2x\dot{x}. \quad (68)$$

This can be rearranged to give an expression for the dynamics in x on the slow manifold:

$$\dot{x} = \frac{\dot{y}}{2x},$$

which is singular for $x = 0$, which coincides with the fold line. This can be desingularised by rescaling time in the whole reduced system by a factor of $2x$. This results in

$$\begin{aligned} \dot{x} &= -(\mu + 1)x - z \\ \dot{y} &= -2x(\mu + 1) - 2xz \\ \dot{z} &= x\mu, \end{aligned} \quad (69)$$

however, it can be noted that the equation for y can be omitted, since the change in y is directly related to the change in x by a factor of $2x$ as stated in equation (68). Therefore, the reduced dynamics can be sufficiently

described by

$$\begin{aligned}\dot{x} &= -(\mu + 1)x - z \\ \dot{z} &= x\mu.\end{aligned}\tag{70}$$

Now, following the theory for folded singularities, the folded node has to satisfy the condition $l(0, 0, z) = 0$

$$\begin{aligned}l(0, 0, z) &= -(\mu + 1)x - z = 0|_{(0, 0, z)} \\ \Rightarrow z &= 0,\end{aligned}$$

which leads to the conclusion that the folded singularity, defined on the slow manifold for $\epsilon \rightarrow 0$ and located on the fold line $L = (0, 0, z)$, is given by $(0, 0, 0)$, as expected. Note that in this case only one equilibrium of the reduced system exists, which is not generally the global case. The next step of the analysis is to verify that the folded singularity at the origin is indeed a folded node. As discussed in the beginning of Section 6, the classification of the singularities is determined by the eigenvalues of the reduced system. Therefore, the next step is calculating these eigenvalues. The Jacobian of the reduced system (70) is

$$J = \begin{bmatrix} -(\mu + 1) & -1 \\ \mu & 0 \end{bmatrix},\tag{71}$$

and therefore the characteristic equation yields

$$\begin{aligned}\sigma^2 + (\mu + 1)\sigma + \mu &= 0 \\ \Rightarrow \sigma_1 &= -1 \quad \text{and} \quad \sigma_2 = -\mu.\end{aligned}$$

Since μ is the eigenvalue ratio and satisfies $0 < \mu < 1$, we can conclude that

$$\sigma_1\sigma_2 = (-1)(-\mu) = \mu > 0,$$

and therefore, by the conditions presented earlier in this Section, this shows that the folded singularity is in fact a folded node. Note that if we had tried to find the eigenvalues for the full three dimensional reduced system (69) instead, an additional eigenvalue $\sigma_3 = 0$ would have occurred. This is the eigenvalue that corresponds to the loss of hyperbolicity at the folded node, which is expected for singular points.

In order to analyse the folded node, the system (??) is transformed using the blow up transformation $u = \epsilon^{1/2}\bar{x}$, $v = \epsilon\bar{y}$, $w = \epsilon^{1/2}\bar{z}$ and $\tau_1 = \epsilon^{1/2}\bar{t}$. Then, in a neighbourhood U of the folded node the system is represented by

$$\begin{aligned}\dot{x} &= \bar{y} - \bar{x}^2 \\ \dot{y} &= \bar{z} - \bar{x} \\ \dot{z} &= -\nu.\end{aligned}$$

In the following analysis, the bars will be omitted for readability. One important realisation is that the phase portraits for the rescaled system is topologically equivalent to the original normal form. Therefore, the mapping of solutions found in the blown up system to the original system is straightforward. ++++check if true++++ All the information needed to describe the dynamics near the fold point is now derived and therefore the next step in the analysis is the description of the SAOs. The SAOs in the folded node case are standard trajectories that follow a certain pattern. These patterns are, as discussed in Theorem 7.1, found by considering the eigenvalue

ratio μ . In the case of the folded node, μ satisfies $2k+1 < \mu^{-1} < 2k+3$. Solving for $k \in \mathbf{N}$, then k is the number of secondary canards ξ_i , where $i \in 1, \dots, k$, in the system as stated in Theorem 7.1. Furthermore, k corresponds to the number of twists the primary canard γ_s is performing around γ_w . A twist corresponds to a 180° rotation, see [?](#). It is important to note that $\mu^{-1} \notin \mathbf{N}$ in order to conclude the number of secondary canards. If $\mu^{-1} \in \mathbf{N}$, bifurcations occur and the number of secondary canards changes. For a full analysis of this phenomenon refer to ([Wechselberger 2005](#)).

These canards are trajectories that are entering the so called funnel region of the fold and contracted along the direction of S^a . This funnel region lies between the fold line L and the strong singular canard. It is represented by the grey region in Figure 17. For decreasing values of ϵ , the funnel becomes narrower and for $\epsilon \rightarrow 0$, all other canards converge to the strong singular canard. The number of SAOs an incoming trajectory undergoes depends on where the trajectory enters the fold region in the z plane. Different intervals I_i , $i \in 1, \dots, k$, of z can be defined according to how many SAOs will be observed in the interval. The interval in which the primary strong canard lies is significantly larger than the other intervals, so the secondary canards close to it will have a higher amplitude while the number of SAOs is smaller. As the number of SAOs increases, the amplitude of oscillations get smaller and are not readily visible. The result about the width of the intervals is summed up in the following theorem.

Theorem 7.2 (Width of Rotational Sectors)

[[Desroches et al. 2012](#)] Consider system (61) and assume it has a folded-node singularity. At an $O(1)$ distance from the fold curve, all secondary canards are in an $O(\epsilon^{(1-\mu)/2})$ neighbourhood of the primary strong canard. Hence, the width of the rotational sectors I_i , $1 \leq i \leq k$, is $O(\epsilon^{(1-\mu)/2})$ and the width of sector I_{k+1} is $O(1)$.

Figure 19: Folded Node Region for $\mu \approx 0.0557$. ([Desroches et al. 2012](#)).

Figure 20: Rotational Sectors for $\mu \approx 0.0557$ ([Desroches et al. 2012](#)).

An illustrative example is provided in ([Desroches et al. 2012](#)), where $\mu \approx 0.0557$ and therefore $k = 8$. Then, besides the strong and weak primary canards γ_s and γ_w , there exist eight secondary canards ξ_i , where $i \in 1, \dots, 8$. Figure....+++ shows a small region of the phase space, which captures the intersection of the repelling and attracting sheet of the slow manifold. This region is bounded by two cross-sections, Σ^a and Σ^{-a} . Another cross-section Σ^{f^n} can be defined, which corresponds to a two dimensional cross-section of the flow at the fold. This is displayed in Figure 19. In the Figure, the primary strong canard is illustrated in black, and the three strongest secondary canards are displayed as ξ_1 in orange, ξ_2 in magenta and ξ_3 in cyan. It is apparent that the primary strong canard makes twists around the center, where the weak canard is located. The secondary canards ξ_i , $i \in 4, \dots, 8$ as well as γ_w are present in the Figure as well. However, they are not visible, since they are increasingly close to each other in the middle.

The number of SAOs a trajectory undergoes is dependent on where it enters the funnel region in terms of the space variable z . The intervals that can be defined are I_0 up to I_9 , where I_0 is bounded by γ_s and much larger than the other intervals. The interval I_i , $i \in 1, \dots, 8$ is bounded by the corresponding number of secondary canards ξ_i to the left and ξ_{i-1} to the right, and entering the fold region through the i th interval corresponds to i oscillations a trajectory undergoes. This is illustrated in Figure 20.

This is only a very local picture of the dynamics present in system (64). Aspects of the global analysis are presented in the following section.

8 Discussion/Conclusion

9 Acknowledgements

Maple (specify release). Maplesoft, a division of Waterloo Maple Inc., Waterloo, Ontario.

References

- Desroches, M., Guckenheimer, J., Krauskopf, B., Kuehn, C., Osinga, H. M. & Wechselberger, M. (2012), ‘Mixed-mode oscillations with multiple time scales’, *SIAM Rev.* **54**(2), 211–288.
URL: <http://dx.doi.org/10.1137/100791233>
- Fenichel, N. (1979), ‘Geometric singular perturbation theory for ordinary differential equations’, *Journal of Differential Equations* **31**(1), 53 – 98.
URL: <http://www.sciencedirect.com/science/article/pii/0022039679901529>
- Festschrift, Broer, H., Krauskopf, B. & Vegter, G. (2001), ‘Global analysis of dynamical systems festschrift dedicated to floris takens for his 60th birthday’. Dedicated To Floris Takens.
- Hek, G. (2009), ‘Geometric singular perturbation theory in biological practice’, pp. 347–386.
- International Technological University (n.d.), ‘7. classification of critical points.’. Date Accessed: 15.12.2018.
URL: <http://staff.www.ltu.se/larserik/applmath/chap9en/part7.html>
- Krupa, M. & Szmolyan, P. (2001), ‘Extending geometric singular perturbation theory to nonhyperbolic points - fold and canard points in two dimensions’, *SIAM J. Math. Analysis* **33**(2), 286–314.
- Kuehn, C. (2015), *Multiple Time Scale Dynamics*, Vol. 191 of *Applied Mathematical Sciences*, Springer International Publishing, Cham.
- Mishchenko, E. (2012), *Differential Equations with Small Parameters and Relaxation Oscillations*, Mathematical Concepts and Methods in Science and Engineering, Springer US.
URL: https://books.google.co.uk/books?id=_UFZmQEACAAJ
- Needham, T. (1998), *Visual Complex Analysis*, Comparative Pathobiology - Studies in the Postmodern Theory of Education, Clarendon Press.
URL: <https://books.google.co.uk/books?id=ogz5FjmiqlQC>
- Strogatz, S. (2007), *Nonlinear Dynamics And Chaos*, Studies in nonlinearity, Sarat Book House, chapter 7, p. 198.
URL: <https://books.google.co.uk/books?id=PHmED2xxrE8C>
- Wechselberger, M. (2005), ‘Existence and bifurcation of canards in R3 in the case of a folded node’, *SIAM Journal on Applied Dynamical Systems* **4**.

A Elements of Dynamical Systems

In this appendix we state some standard results from dynamical systems theory.

A.1 Stable Manifold Theorem

Suppose $\dot{x} = F(x)$ where $x \in \mathbf{R}^n, F \in C^r(\mathbf{R}^n, \mathbf{R}^n)$ and has only hyperbolic fixed points (i.e. in the associated linearised system $\dot{x} = Ax, A \in \mathbf{R}^n$ has no eigenvalues λ such that $\text{Re}(\lambda) = 0$).

A.2 Centre Manifold Theorem

A.3 Implicit Function Theorem

A.4 Hartman Grobman Theorem

DO we need this?

A.5 Hopf Bifurcations

B Numerical Simulation

Many figures in this document? were produced using MATLAB, for example: fig ++++++. In this appendix, we will give a brief tutorial on their production. Fast-slow systems like the ones studied here are a classic example of *stiff* ODEs^a.

Definition B.1 (Stiffness Ratio). *Consider $\dot{x} = F(x)$ where $x \in \mathbf{R}^n, F \in C^r(\mathbf{R}^n, \mathbf{R}^n)$. Let*

$$\dot{x}' = Ax, \quad A \in \mathbf{R}^{n \times n}$$

denote its linearisation. Suppose all the eigenvalues λ_j of A have negative real parts. Then the stiffness ratio, μ is defined as

$$\mu := \frac{\max_j(\text{Re}(\lambda_j))}{\min_j(\text{Re}(\lambda_j))}$$

If μ is large, the system is called stiff.

Stiffness is not a well-defined concept, it can be seen as a general term for a set of equations which are difficult to solve numerically to a high level of accuracy. Throughout this section we will consider the general problem above as an initial value problem.

$$\begin{cases} \dot{x} = F(x) \\ x(T_0) = x_0 \end{cases}$$

As before, $x \in \mathbf{R}^n$ and $F \in C^r(\mathbf{R}^n, \mathbf{R}^n)$. To solve such a system numerically, time must be discretised. Using standard notation, let h be the time step between points on the solution. To differentiate between the continuous solution $x(t)$ and the discretised solution, we denote the latter by $x(t_j) = x_j$. Here $t_j = T_0 + jh$. As a first example, consider the modified Euler method.

^aIndeed, the MATLAB documentation for its stiff solver, `ode15s`, uses the Van Der Pol equation as it's example.

$$x(t_{n+1}) = x(t_n) + hF \left(x(t_n) + \frac{1}{2}F(x(t_n)) \right)$$

Or, in the more compact notation,

$$x_{n+1} = x_n + hF \left(x_n + \frac{1}{2}F(x_n) \right)$$

This is a simple method and provides a starting point in considering error between true and numerical solutions.

The go-to ODE solver in MATLAB is `ode45`. This function uses the Dormand-Prince Runge-Kutta method, an explicit single-step formula. The Runge-Kutta method (RK4) is similar to the explicit Euler method in that it calculates the next point (x_{n+1}) using only its current value (x_n). Unlike the Euler method however, it yields much lower error by using a better approximation of the derivative at points in between x_n and x_{n+1} as opposed to only the derivative at the initial point. The Runge-Kutta method uses the following relation.

$$x_{n+1} = x_n + \frac{1}{6}h(k_1 + 2k_2 + 2k_3 + k_4)$$

where

$$\begin{aligned} k_1 &= F(x_n) \\ k_2 &= F \left(x_n + \frac{1}{2}hk_1 \right) \\ k_3 &= F \left(x_n + \frac{1}{2}hk_2 \right) \\ k_4 &= F(x_n + hk_3) \end{aligned}$$

The Runge-Kutta family of solvers are ubiquitous in numerical analysis, and most methods can be categorised as belonging to this set of methods. Even the simplest, the explicit Euler scheme, is a RK method. Note that `ode45` doesn't use RK4, it uses an adaptive method that repeats steps if the error in the step is too high. This produces an even more accurate solution without adding much computational cost.

Let's look at the use of these various methods on the simplest fast-slow system.

$$\begin{cases} \begin{pmatrix} \dot{x} \\ \dot{y} \end{pmatrix} = \begin{pmatrix} -1/\epsilon & 0 \\ 0 & -1 \end{pmatrix} \begin{pmatrix} x \\ y \end{pmatrix} \\ (x(0), y(0)) = (x_0, y_0) \end{cases} \quad (72)$$

This system has an easy analytic solution, $x(t) = x_0 \exp(-t/\epsilon)$, $y(t) = y_0 \exp(-t)$. For this reason it is a useful test system with which to analyse the convergence of numerical schemes. The stiffness ratio for this system is

$$\mu = \frac{\max_j(\operatorname{Re}(\lambda_j))}{\min_j(\operatorname{Re}(\lambda_j))} = \frac{1}{\epsilon}$$

The time separation, $\epsilon \ll 1$ and so this system is very stiff. We thus expect explicit solvers to perform poorly. +++Explain about convergence here? Would be nice to do for modEuler and RK4 too+++.

The lack of stability of these algorithms in practice, even for very simple systems, clearly necessitates the introduction of alternative methods.

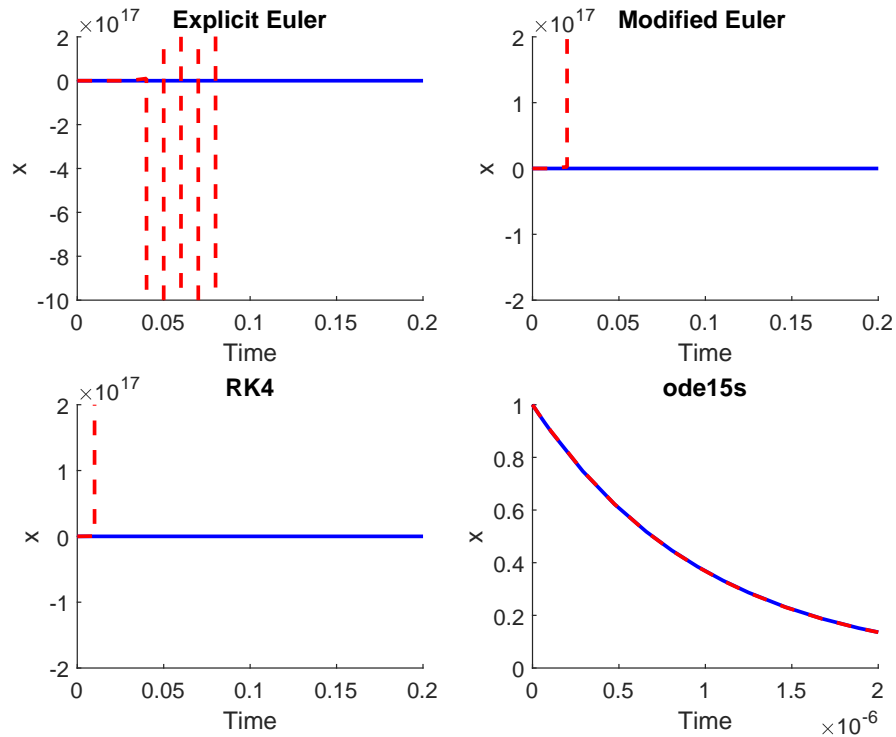


Figure 21: Comparison of stability of different numerical schemes applied to Equation 72. Blue solid line indicates analytic solution, dashed red indicates numeric solution using the scheme given in the plot title. Note the varying scales on the axes.

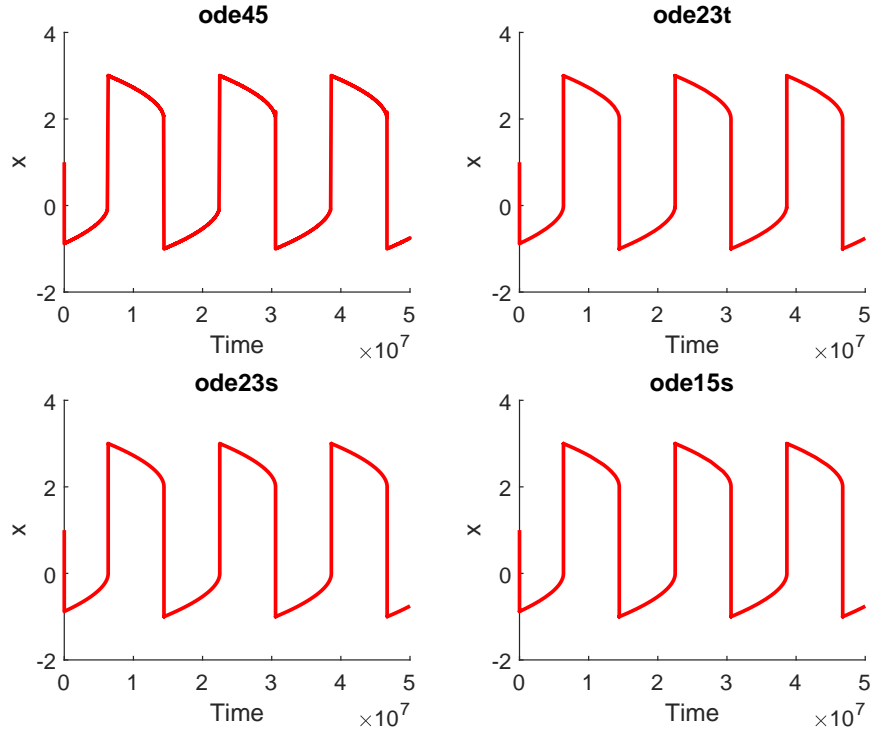


Figure 22: Comparison of stiff solvers for VDP. Note all get correct trajectory, what about speed?++.

B.1 Stiff Solvers

+++`ode15s`,`ode23t`,`ode23s` use, comparison of speed with `ode45`. Note difference between RK4.+++
Test on RK4, mod-Euler and `ode15s`? Intro BDF? Check sec8 MMO.

C Dynamics in K_2